Accepted for publication in the Bulletin of the Seismological Society of America on 18th July 2022

Construction of a Ground-Motion Logic-Tree Through Host-to-Target Region Adjustments Applied to an Adaptable Ground-Motion Prediction Model

David M. Boore*[1], Robert R. Youngs[2], Albert R. Kottke[3], Julian J. Bommer[4], Robert Darragh[5], Walter J. Silva[5], Peter J. Stafford[4], Linda Al Atik[6], Adrian Rodriguez-Marek[7], and James Kaklamanos[8]

1. Consultant, Los Altos, CA, USA
2. Wood Environment & Infrastructure Solutions, Inc., Oakland, CA, USA
3. Pacific Gas & Electric Company, San Francisco, CA, USA
4. Dept. of Civil and Environmental Engineering, Imperial College London, London SW7 2AZ, UK
5. Pacific Engineering & Analysis, El Cerrito, CA 94530, USA
6. Al Atik Consulting, San Francisco, CA, USA
7. Department of Civil and Environmental Engineering, Virginia Tech, Blacksburg, VA, USA
8. Department of Civil Engineering, Merrimack College, North Andover, MA, USA

*Corresponding author: dboore@yahoo.com

ABSTRACT

The purpose of a median ground-motion logic-tree is to capture the center, body, and range of possible ground-motion amplitudes for each earthquake scenario considered in a seismic hazard analysis. For site-specific hazard analyses, the traditional approach of populating the logic-tree branches with ground-motion prediction models (GMPMs) selected and weighted on the basis of vaguely defined applicability to the target region is rapidly being abandoned in favor of the backbone GMPM approach. In this approach, the selected backbone model is first adjusted to match the earthquake source and path characteristics of the target region, and then it is separately adjusted to account for the site-specific geotechnical profile. For a GMPM to be amenable to such host-to-target adjustments, the magnitude scaling of response spectral ordinates should be consistent with the theoretical scaling of Fourier amplitude spectra. Additionally, the influence of

individual source and path parameters should be clearly distinguished in the model to allow the adjustments to be applied individually, and reliable estimates of the source and path parameters from the host region of the GMPM should be available, as should a reference rock profile for the model. The NGA-West GMPM of Chiou and Youngs (2014) (CY14) has been identified as a very suitable backbone model. Moreover, rather than adopting generic source and path parameters and a rock site profile from the host-region for CY14—which is not easily defined since the data from which it was derived come from several geographical locations—recent studies have inverted the model to obtain a CY14-consistent reference rock profile and CY14-compatible source and path parameters. Using these host-region characteristics, this study illustrates the process of building a ground-motion logic-tree through the sequential application of multiple host-to-target region adjustments, each represented by a node on the logic tree to achieve a tractable model for the total epistemic uncertainty.

INTRODUCTION

Logic trees are used ubiquitously in probabilistic seismic hazard analysis (PSHA) to incorporate epistemic uncertainty in each of the elements of the models characterizing seismic sources and ground motions. The fundamental objective of logic trees is to capture the center, the body, and the range (CBR) of technically defensible interpretations (TDI) of the available data, methods, and models (USNRC, 2018). For ground-motion characterization (GMC) models, this translates into defining, for each earthquake scenario specified by the seismic source characterization (SSC) model, the full distribution of possible ground-motion amplitudes. Constructing GMC logic-trees by populating the branches with published ground-motion prediction models (GMPMs), selected on the basis of their applicability—inferred or tested using local data, often from small-magnitude earthquakes—is unlikely to capture the CBR of TDI. Even in regions with abundant ground-motion data, the published GMPMs are not considered to adequately capture the full range of epistemic uncertainty (e.g., Al Atik and Youngs, 2014), and it is very unlikely that the published GMPMs will capture the range when applied to the target region. Moreover, there is a fundamental problem in the traditional approach of populating the logic-tree branches with published GMPMs, namely that the relationship between the weights on the models and the weights on the resulting distributions of ground-motion amplitudes is opaque. All of these considerations have given rise to alternative techniques, collectively called the ‘backbone

GMPM' approach (Bommer, 2012), in which the branches of the GMC logic-tree are populated by scaled versions of a single backbone GMPM (e.g., Atkinson et al., 2014). A key part of the backbone GMPM approach is that weights are assigned to logic-tree branches to reflect the relative degree of confidence in each alternative model or parameter value; these weights are subsequently treated as probabilities in the calculation of the mean hazard and the associated fractiles. This requires the alternative branches at each node to satisfy the MECE (mutually exclusive and collectively exhaustive) criterion (e.g., Bommer and Scherbaum, 2008), which is unlikely to be the case using multiple GMPMs derived from overlapping datasets, whereas using the backbone approach, the logic-tree branches will inevitably be mutually exclusive.

Using only published GMPMs from a different (host) region will seldom capture the center of the distribution, because the host and target regions are rarely, if ever, perfect analogs. Moreover, published GMPMs, with generic site amplification factors conditioned on parameters such as V_{S30} (time-averaged shear-wave velocity in the upper 30 m of the subsurface) and $Z_{1.0}$ or $Z_{2.5}$ (depths to shear-wave velocity horizons of 1.0 km/s and 2.5 km/s, respectively), are very unlikely to capture the dynamic response characteristics of the target site. For these reasons, the development of a site-specific GMC logic-tree will generally require host-to-target adjustments to render each GMPM more applicable to the target region and site. Within the backbone framework, the adjustments for differences in source, path, and site characteristics between the host region of the GMPM and the target region and site of the PSHA provides a tractable way to develop the distribution of epistemic uncertainty by assigning branches for the uncertainty in the estimates of each variable for which the adjustments are made.

When a GMC logic-tree is to be constructed by applying a series of host-to-target adjustments to a backbone GMPM, the emphasis in selecting the backbone model shifts from seeking a model that is in some sense applicable to the target region to identifying a model that is amenable to being adjusted to match the target-region characteristics. An adaptable GMPM can be broadly defined as one in which the influence of each individual source and path parameter is clearly identifiable and isolated, and in which the scaling of response spectral accelerations with magnitude is consistent with the theoretical scaling based on Fourier amplitude spectra in stochastic simulations (Boore, 2003). Bommer and Stafford (2020) identified the NGA-West2

model of Chiou and Youngs (2014)—hereafter CY14—as the most adaptable GMPM for shallow crustal seismicity because its formulation is most consistent with seismological theory.

To apply the host-to-target adjustments, estimates are needed for the source, path, and site parameters of the host region where the backbone GMPM was developed, and for the target region and site for which the PSHA is being conducted. When applying such hybrid-empirical adjustments, it has been common practice to compile host-region parameters from seismological studies conducted in the region represented by the backbone GMPM (e.g., Campbell, 2003). A preferable approach, especially for models such as the NGA-West2 GMPMs that are derived from a dataset compiled from several active crustal regions, is to determine a suite of source, path, and site parameters that collectively optimize the match of the output from stochastic simulations with the predictions from the GMPM over the ranges of magnitude and distance of greatest relevance to the PSHA calculations (e.g., Scherbaum et al., 2006). Using the host crustal shear-wave velocity (V_S) profile and high-frequency attenuation (kappa) value determined for the CY14 GMPM by Al Atik and Abrahamson (2021), Stafford et al. (2022) have determined a suite of source and path parameters for the effective host-region of the CY14 GMPM, which provide the starting point for any application using this model as a backbone GMPM.

The purpose of this article is to illustrate the process of applying multiple host-to-target adjustments to the CY14 backbone GMPM to construct a GMC logic-tree for PSHA. The target location is the Idaho National Laboratory (INL), where a SSHAC (Senior Seismic Hazard Analysis Committee) Level 3 PSHA (Ake et al., 2018) is currently underway. The adjustments are illustrated only for source and path parameters, consistent with the development of the GMC model for PSHA, which is incorporating site response effects using the convolution approach of Bazzurro and Cornell (2004), usually referred to as Approach 3 (McGuire et al., 2001). Traditionally, this approach has involved adjusting the GMPMs to a buried reference rock horizon, and then convolving the hazard at this horizon with the amplification factors for the overlying layers, effectively applying the site adjustment in two steps (e.g., Rodriguez-Marek et al., 2014). In the INL PSHA project, in common with other recent projects, the hazard calculations are conducted using the source- and path-adjusted backbone GMPM but retaining the host reference rock profile. The site adjustments are then applied in a single step, using the ratio of the amplification factors for the full crustal profiles for the target site to those for the host

reference rock profile anchored to a V_{S30} of 760 m/s. For a discussion of this alternative one-step approach, the reader is directed to the report by Rodriguez-Marek, Ake, et al. (2021).

This article begins with an overview of the CY14 model, identifying the individual terms to be adjusted. Then the article describes two adjustments which may be required for the CY14 model that are not region-specific but rather related to features of how this model was derived. The first adjustment corresponds to the long-period response spectral ordinates, recognizing the approach adopted by Chiou and Youngs (2014) regarding usable data at long periods was unique among the NGA-West2 models, all of which predict systematically larger accelerations at long (> 5 seconds) periods. The second adjustment corresponds to the scaling for normal-faulting earthquakes, which is relevant to the INL study since the site is located with the Basin and Range extensional province. The dataset used to derive the CY14 model contained very few recordings from normal events, for which reason scaling for this type of rupture is uncertain due to the poor constraint.

The adjustments for source (stress parameter, $\Delta\sigma$) and path (anelastic attenuation quality factor, Q) parameters representative of the INL region are then presented, including the estimation of the target-region values and their associated uncertainty. For each adjustment, we discuss example weights of the logic-tree branches used to capture the epistemic uncertainty of the adjustments. The logic-tree branches and the weights for all the adjustments considered in this article are given in the final figure of the main body of this article.

This article concludes with a brief discussion of how the resulting range of epistemic uncertainty could be evaluated and the options for broadening the distribution, if required.

The intent of this article is to demonstrate the process of possible adjustments to a well-known backbone GMPM. The results are not intended for direct application, so unless needed as part of the exposition, tables of coefficients are not provided.

THE CY14 EQUATIONS AND TERMS TO BE ADJUSTED

For the purposes of this article, it is useful to break the CY14 function for the reference rock motion (y_{ref}) into parts that represent the different physical processes that contribute to the ground motion, as in equation (1):

$$\ln y_{ref} = F_C + F_{SoF} + F_S + F_{GS} + F_A + F_{Ztor} + F_{Dip} + F_{DPP} + F_{HW}, \quad (1)$$

where the terms are functions for the effects of style-of-faulting (F_{SoF}), source (F_S), geometrical spreading (F_{GS}), path (F_A), depth to top of rupture (F_{Ztor}), fault dip (F_{Dip}), directivity (F_{DPP}), and hanging wall (F_{HW}); F_C is a metadata-independent function. Equation (1) gives the motion for a reference rock condition ($V_{S30} = 1130$ m/s in CY14). Because they use metadata that are most used in applications, and for which it is possible to make adjustments from analysis of data in the INL region, we consider only the first five terms in this article. They are defined by the following equations:

$$F_C = c_1 \quad (1a)$$

$$F_{SoF} = \left\{c_{1a} + \frac{c_{1c}}{\cosh[2\max(\mathbf{M} - 4.5, 0)]}\right\} F_{RV} + \left\{c_{1b} + \frac{c_{1d}}{\cosh[2\max(\mathbf{M} - 4.5, 0)]}\right\} F_{NM} \quad (1b)$$

$$F_S = c_2(\mathbf{M} - 6) + \frac{c_2 - c_3}{c_n}\ln\left[1 + e^{c_n(c_M - \mathbf{M})}\right] \quad (1c)$$

$$F_{GS} = c_4 \ln\{R_{RUP} + c_5 \cosh[c_6 \max(\mathbf{M} - c_{HM}, 0)]\} + (c_{4a} - c_4)\ln\left(\sqrt{R_{RUP}^2 + c_{RB}^2}\right) \quad (1d)$$

$$F_A = \gamma R_{RUP} \quad (1e)$$

where γ is an anelastic attenuation parameter given by

$$\gamma = c_{\gamma 1} + \frac{c_{\gamma 2}}{\cosh\left[\max\left(\mathbf{M} - c_{\gamma 3}, 0\right)\right]} \quad (1f)$$

In these equations, **M** is moment magnitude; R_{RUP} is rupture distance; F_{RV} and F_{NM} are indicator variables for reverse and normal faulting, respectively; and all *c* parameters (with various subscripts) are model coefficients. The definitions of the other four terms (F_{Ztor}, F_{Dip}, F_{DPP}, and F_{HW}) can be inferred by comparing the definitions in equation (1) with equation (11) of CY14. The effects of site conditions are given in equation (12) of CY14, and CY14 should be consulted for the definitions of the coefficients appearing in equation (1). Period dependence is implicit in the functions. Also note that all but F_C are dependent on metadata of some sort (style of faulting, depth to top of rupture, fault dip, magnitude, distance measures).

The physical processes that are most likely to produce regional-dependent differences in the ground motion are: 1) the amplitude and frequency content radiated from the earthquake sources and 2) the effect of propagation from the source to the site. These contributors to the ground shaking are represented by F_S for the source and F_{GS} and F_A for the path. The path dependence is separated here into geometrical spreading and anelastic attenuation, respectively, for convenience in later discussions. For reasons discussed in the section on F_A, we only consider host-to-target path adjustments for F_A and not F_{GS}.

All adjustments to a backbone GMPM can have epistemic uncertainties. One of the advantages of the CY14 GMPM is that these uncertainties can be taken into account by branches in a logic tree. We illustrate how this can be done for four functions in the CY14 GMPM for which we discuss adjustments: the metadata-independent function F_C, the style-of-faulting function F_{SoF}, the source function F_S, and the path function F_A.

NON-REGIONALLY DEPENDENT ADJUSTMENTS

F_C, Metadata-Independent Function

Chiou and Youngs (2008) found period-to-period discontinuities in the coefficient c_1 at longer periods that matched drops in the number of usable records due to filtering, from which they concluded that the long-period estimates of c_1 are biased to stronger motions; they removed this

bias by imposing a smooth variation in the slope of c_1 with respect to period. This was a post-regression adjustment. Consequently, CY14 tends to predict lower long-period ordinates relative to the other NGA-West2 models, as shown in Figure 1. To define the epistemic uncertainty, an adjustment to CY14 can be made for the long periods, and this adjustment can be given a weight in a branch of the logic tree. A method for defining the adjustment is as follows. Examples of the steps for **M** = 6.5 are shown in Figure 2.

- Compute the 5%-damped pseudo-acceleration response spectra (PSA) from four NGA-West2 GMPMs for R_{RUP} from 1 to 100 km, **M** from 5 to 8, and strike-slip (SS) earthquakes for a set of 22 oscillator periods with spacing from 0.008 s to 10 s. The period spacing is approximately logarithmic.

- Calculate the geometric mean of the PSA, $\mathrm{PSA_{GMEAN}}$, from Abrahamson et al. (2014) (ASK14), Boore et al. (2014) (BSSA14), and Campbell and Bozorgnia (2014) (CB14) for each set of **M**, R_{RUP}, and spectral period T.

- Calculate $\ln(\mathrm{PSA_{GMEAN}}/\mathrm{PSA_{CY14}})$, where $\mathrm{PSA_{GMEAN}}$ is computed in the previous step and $\mathrm{PSA_{CY14}}$ is the PSA for CY14 evaluated for the set of **M**, R_{RUP} and T; the result is shown in Figure 2a.

- For each **M** and R_{RUP}, fit the period-dependent function $C + \Delta c_1$ to $\ln \frac{\mathrm{PSA_{GMEAN}}}{\mathrm{PSA_{CY14}}}$, where C is a period-independent constant and Δc_1 is an adjustment term given by

$$\Delta c_1 = S \times \max\left\{\ln\left(\frac{T}{T_B}\right), 0\right\}^2 \qquad (2)$$

  where T_B is a magnitude-dependent threshold period given by $T_B = 2 - \max(0, \mathbf{M} - 7)$; $\Delta c_1 = 0$ for periods less than T_B. Δc_1 is plotted in Figure 2b for six distances and $\mathbf{M} = 6.5$.

The *S* in equation (2) depends on distance and magnitude, as given in the following four equations:

$$S = S_1 + \frac{S_2}{\cosh(S_3 \times R_{RUP})} \quad (3)$$

$$S_1 = 0.4050 - 0.1989 \times \max(\mathbf{M} - 7, 0) \quad (3a)$$

$$S_2 = -0.2413 + 0.1587 \times \max(\mathbf{M} - 7, 0) \quad (3b)$$

$$S_3 = 0.1474 + 0.0261 \times \max(\mathbf{M} - 7, 0) \quad (3c)$$

The adjusted function for F_C thus becomes

$$F_C = c_1 + \Delta c_1 \quad (4)$$

The logic tree for F_C has 2 branches, one with $\Delta c_1 = 0$ and one with Δc_1 given by equation (2). It is reasonable to use weights of 0.5 for each branch as a default condition. On the other hand, it could be argued that there were good reasons for CY14 to expect a long-period bias and that the other three GMPMs (ASK14, BSSA14, and CB14) are not independent in that they used similar data and did not consider a post-regression adjustment for a bias in the long-period PSA. In this case, more weight could be given to the branch for which $\Delta c_1 = 0$.

F_{SoF}, Style-of-Faulting Function

Of the 300 earthquakes in the database used to derive CY14, only 8 were normal-slip events. The constraint on the coefficients for scaling for normal-slip earthquakes is therefore rather weak. One way to address this issue is to look at the relative scaling of spectral accelerations for normal-slip (NS) to strike-slip (SS) earthquakes in several current GMPMs, and use these to infer possible adjustment factors to be applied to the F_{NM} term in equation (1b). Figure 3a shows the NS/SS ratio for several recent GMPMs, including four of the NGA-West2 GMPMs and two models (Akkar et al., 2014a,b [Aea14,a,b] and Bindi et al., 2014a,b [Bea14a,b]) based largely on Pan-European data, with relatively more NS events than used in the NGA-West2 GMPMs. Not shown in Figure 3a is the NS/SS ratio from a recent GMPM using data from Greece (Boore et al., 2020); the ratio for this model is very similar to that shown in Figure 3a for BSSA14, particularly for periods less than about 2 s. More than 50 NS earthquakes provided data used in the Boore et al. (2020) GMPM. The BSSA14 values are also similar to NS/SS ratios of 0.8 for peak acceleration (PGA) and 0.85 for peak velocity (PGV) for Greece, from equations (3a) and (4a) in Skarlatoudis et al. (2003), assuming that PGA and PGV are similar to PSA at periods of

0.01 and 1.0 s, respectively. There is considerable variation in the NS/SS ratio, as shown in Figure 3a, although three of the four NGA-West2 models are similar for periods less than about 1 s. A convenient way to capture some of the uncertainty shown in Figure 3a is to multiply F_{NM} by a factor α_{NM}, where that factor is defined as follows:

- $\alpha_{NM} = 1$. No change to CY14 scaling; consistent with 3 NGA-West2 models (at short periods) although all are deficient in normal-faulting data.
- $\alpha_{NM} = 0$. Implies no difference between NS and SS motions; consistent with the Bea14a,b and Spudich et al. (1996; 1999, with an erratum given by Spudich and Boore, 2005) GMPMs for extensional regions.
- $\alpha_{NM} = \frac{1}{2}$. Model that lies between these two end members; consistent with ASK14 (at short periods) and Aea14a,b.

The adjusted NS/SS ratios for the CY14 GMPM using these factors are shown in Figure 3b for two magnitudes (note that the ratio is unity when $\alpha_{NM} = 0$ and therefore is independent of magnitude).

The adjusted function for F_{SoF} is given by equation (4):

$$F_{SoF} = \left\{c_{1a} + \frac{c_{1c}}{\cosh[2\max(\mathbf{M} - 4.5, 0)]}\right\} F_{RV} + \left\{c_{1b} + \frac{c_{1d}}{\cosh[2\max(\mathbf{M} - 4.5, 0)]}\right\} \alpha_{NM} F_{NM} \quad (4)$$

No adjustment is included for the F_{RV} term because there are no reverse-slip earthquakes for the target region used in this article.

With the formulation in this section, there are three logic-tree branches, corresponding to $\alpha_{NM} =$ 0, ½, and 1. As most of the GMPMs predict NS motions to be less than SS motions (Figure 3a), it is reasonable to give less weight to the $\alpha_{NM} = 0$ branch than the other two branches. A possible set of weights is 0.2, 0.4, and 0.4 for the $\alpha_{NM} = 0$, ½, and 1 logic-tree branches, respectively.

REGIONALLY DEPENDENT ADJUSTMENTS

Regionally dependent adjustments are made to the F_S and F_A functions. The adjustments use parameters obtained from inversions of ground-motion data recorded in the target region. Before describing the adjustments, we first discuss briefly the target region data and the inversion process.

Data

The data used in the inversions are Fourier amplitude spectra (FAS) computed from data recorded by a number of networks, including U.S. Geological Survey networks, INL Seismic Monitoring Program, Intermountain West Seismic Network, US National Seismic Network, University of Utah Regional Seismic Network, and the USArray Transportable Array. The data included horizontal-component records from accelerometers and broadband instruments (as well as a few short-period instruments). The data were processed uniformly, using the procedures developed for use in various NGA projects; the processing procedures are described in Ancheta et al. (2014). The logarithmically smoothed, vector-summed FAS from each recording used in the inversions have been adjusted for estimates of the smoothed site response, as described in the next paragraph. Details about the data selection, processing, and site amplifications are in Silva et al. (2021). The magnitude-distance distribution resulting from the selection process is shown in Figure 4. Data both inside (shown by squares in the figure) and outside the INL footprint were used. It is clear that the bulk of the data are for earthquakes less than magnitude 5, at distances beyond 100 km. On the other hand, except for long periods, most of the seismic hazard at INL comes from earthquakes greater than magnitude 5 and distances less than 100 km. Because the available data are not for the hazard-significant magnitudes and distances, there will be significant epistemic uncertainty in the adjustment factors.

Estimated site amplifications were removed from the FAS before they were used in the inversion process. The theoretical site amplifications for seven INL sites were computed using measured shear-wave velocity profiles at those sites, after removal of any near-surface soil layers. The amplifications were smoothed over frequency before they were used to adjust the FAS. The

amplifications for the sites without a velocity profile were based on the similarity of empirical site terms, determined from mixed effects regression analysis, with the empirical site terms at the seven INL stations. Cluster analysis was used to group sites with similar empirical site terms, and these groups were related to one of the seven INL sites on the basis of the closeness to one another on a Sammon's map (e.g., Scherbaum et al., 2010; Goulet et al., 2018). More details concerning the estimation of site amplifications are in Silva et al. (2021).

Inversion Process

The adjustments to the CY14 backbone GMPM are based on parameters that describe the Fourier acceleration spectra (FAS) of the target-region data. The parameters were obtained using Markov chain Monte Carlo (MCMC) methods in a three-step process. The MCMC method is used because of its flexibility while also including information through Bayesian inference and prior distributions. The starting model used the Stafford et al. (2022) (Sea22) optimal model parameters.

- Solve for the event-specific stress parameters ($\Delta\sigma$, the parameter controlling the amplitude of high-frequency radiation from the source; see Boore, 1983), the parameters describing the Q model, and the site-specific kappa (κ_0) attenuation parameter (to a first approximation, κ_0 is presumed to be the value of the high-frequency spectral decay parameter κ at zero distance, because the frequency-dependent attenuation of motion with distance has been accounted for by the Q model).
- Using the site-specific κ_0 values from the previous step, fit the model again to obtain $\Delta\sigma$ and the Q model.
- Using the site-specific κ_0 from step 1 and the Q model from step 2, solve for the event-specific stress parameters $\Delta\sigma$.

A common challenge in the development of ground-motion models is the potential for parameters to trade-off with one another. This is especially the case when data are available in only a limited range of the domain (e.g., small range of distances). The procedure listed above

incrementally inverts for the parameters to isolate the influence of the specific parameter. The resulting stress parameters and Q model are discussed in the following sections.

F_S, Source Function

Appendix A shows that F_S can be easily modified to account for differences in host- and target-region stress parameters $\Delta\sigma$. The modified equation for F_S is given by equation (A4), repeated here:

$$F_S = c_2(\mathbf{M} - 6) + \frac{c_2 - c_3}{c_n}\ln\left[1 + e^{c_n(c_M + \Delta c_M - \mathbf{M})}\right] - (c_2 - c_3)\Delta c_M \quad (5)$$

where the difference in the coefficient c_M for the two regions (Δc_M) is related to the ratio of the stress parameters for the regions, as given by equation (A19) in Appendix A, repeated here for convenience:

$$\Delta c_M = \chi_{FS2RS}\frac{2}{3}\log\frac{\Delta\sigma_2}{\Delta\sigma_1} \quad (6)$$

where "1" and "2" refer to the host- and target-regions, respectively, and χ_{FS2RS} is a period-dependent factor (given in Appendix A) that accounts for differences in the slopes of the magnitude scaling for Fourier spectra (FS) and response spectra (RS). Stafford et al. (2022) inverted the CY14 GMPM to determine various parameters that can be used to predict the FAS in the host region. (The base-10 logarithm is used in equation (6) because it comes from a derivation that uses the standard relation between seismic moment and moment magnitude given in equation (A7), which is in terms of the base-10 logarithm; the rest of the logarithms in this article, denoted by the notation "ln", are base-*e* logarithms.) The parameters determined by Sea22 include $\Delta\sigma_1$ and path parameters (used in the section discussing adjustments to F_A). Sea22 found that $\Delta\sigma_1$ increases with **M** up to **M** = 5.0, after which it is constant. We assume that the same dependence occurs in the target region. The finding that the stress parameter is constant for $\mathbf{M} \geq 5.0$ is convenient, because most PSHAs in tectonically active areas use a minimum magnitude of 5.0, and therefore complications due to magnitude-dependent $\Delta\sigma$ can be avoided.

To obtain $\Delta\sigma_2$, we inverted FAS from data recorded in the region surrounding the INL discussed earlier. The inverted stress parameters are plotted against magnitude in Figure 5. Also included in that figure is a bilinear fit to the data, assuming the same functional dependence between $\Delta\sigma$ and **M** used in Sea22, but ignoring the depth dependence in the Sea22 equation. The function used in this article is given by equation (7).

$$\ln \Delta\sigma = s_\alpha + s_\beta \min(\mathbf{M} - 5, 0), \tag{7}$$

where s_α and s_β are regression coefficients. We could use $\exp(s_\alpha)$ as $\Delta\sigma_2$ in equation (6), but there is so much scatter in the inverted stress parameters that a more sophisticated approach is needed. We used the following steps:

- Simulate many (4000 in this article, as the computations are very rapid) datasets of $\Delta\sigma$ values for the earthquakes used to obtain the stress parameters shown in Figure 5, where for each dataset, the stress parameter for each event is generated randomly from a log-normal distribution, using the mean and standard error of the stress parameters from the inversion of the actual data.
- For each simulated dataset:
  - Fit equation (7) to the simulated values of $\Delta\sigma$.
  - Let $\Delta\sigma_{\mathbf{M5}}$ denote the stress parameter for earthquakes with $\mathbf{M} \geq 5$. For a range of stress parameters $\Delta\sigma_{\mathbf{M5}}$ from 20 to 300 bars, compute the probability p that each value of $\Delta\sigma_{\mathbf{M5}}$ would be less than or equal to the value expected from a normal distribution with a mean of s_α and a standard deviation given by the standard error of s_α. This gives the cumulative distribution function (CDF) of $\Delta\sigma_{\mathbf{M5}}$ for each simulated dataset. As shown in Figure 6, this range was sufficient to define the CDF from 0 to 1.
- Compute the mean of p over the 4000 datasets for each value of $\Delta\sigma_{\mathbf{M5}}$. This gives the average CDF for $\Delta\sigma_{\mathbf{M5}}$.
- Sample the CDF using the 5-point Miller and Rice (1983) approximation to the CDF derived in the previous step.

Using the procedure given above, the cumulative distribution functions (CDF) of $\Delta\sigma_{\mathbf{M5}}$ for both the host region (computed from the Sea22 mean and standard error of $\Delta\sigma_{\mathbf{M5}}$) and the target

region (from the procedure discussed in the bulleted list above) are shown in Figure 6 as a function of $\Delta\sigma_{\mathbf{M5}}$. The horizontal dashed lines are the CDF values used in the 5-point Miller and Rice (1983) approximation of the $\Delta\sigma_{\mathbf{M5}}$ CDF, and the vertical dashed lines are the corresponding $\Delta\sigma_{M5}$ values for the target region (to avoid clutter, the vertical lines for the host region CDF are not shown). The resulting discrete values of $\Delta\sigma_{\mathbf{M5}}$ from the host-region and the target-region inversions are used as $\Delta\sigma_1$ and $\Delta\sigma_2$, respectively, in computing Δc_M using equation (6). The Δc_M values are used with appropriate weights in the logic tree to capture the uncertainty in F_S. The results, including the logic-tree weights for the five branches, are given in Table 1 for an oscillator period of 0.1 s. To give an idea of the relation of the epistemic uncertainty in $\Delta\sigma_{\mathbf{M5}}$ to the scatter in the inverted stress parameters, $\Delta\sigma_{\mathbf{M5}}$ for the lowest, middle, and highest logic-tree branches have been added to the plot of the $\Delta\sigma$ in Figure 5. The weights of the logic-tree branches are such that they and the associated values of $\Delta\sigma_{\mathbf{M5}}$ are a discrete representation of the continuous CDF for the host-region and the target-region; those values of $\Delta\sigma_{\mathbf{M5}}$ are used to compute the Δc_M values, and therefore the logic-tree branches for Δc_M have the same weights as the discrete $\Delta\sigma_{\mathbf{M5}}$ values.

The F_S source function for the host- and target-region are plotted against **M** in Figure 7, for a period of 0.1 s. It is clear that the epistemic uncertainty in $\Delta\sigma_{\mathbf{M5}}$ leads to a large range in PSA values (but branches 1 and 5 have lower weights than branch 3, as shown in Figure 5 and in Table 1).

F_A, Path Function

We only consider host-to-target path adjustments for F_A and not F_{GS}. We do this because F_A and F_{GS} are correlated, such that various combinations can result in similar motions at distances that matter in engineering applications. With the available ground-motion datasets, it is difficult to isolate the two components independently. On the other hand, F_A has little effect on ground motions at short to intermediate distances, so the usual approach in building GMPMs is to use data at those distances to determine F_{GS} and then use that function at all distances, with F_A being determined by more distant data. Recent GMPMs that allow for regional differences in the path effect on ground motions (e.g., ASK14, BSSA14, CB14, and CY14) assume that F_{GS} is region-independent, with regional differences in the path function being accounted for only in F_A.

The adjustments to F_A (equation (1e)) were derived by comparing simulated response spectra for models of the target-region and the host-region FAS, focusing on the parameters that control the attenuation with distance. The host-region FAS model comes from Sea22, whereas the target-region FAS uses the Sea22 geometrical spreading, with a target-region anelastic attenuation model Y as parameterized by the function in equation (8):

$$Y = \exp\left[-(\pi f R_{RUP})/\left(Q c_Q\right)\right], \tag{8}$$

where f is frequency, and c_Q is a shear-wave velocity, taken as 3.5 km/s both in Sea22 and in this article. Q is the attenuation quality factor, given by

$$Q = Q_0 f^{\eta(\mathbf{M})}, \tag{9}$$

where Q_0 is a regression parameter, and the magnitude-dependent exponent $\eta(\mathbf{M})$ is given by

$$\eta(\mathbf{M}) = \eta_\alpha + \eta_\beta \tanh\left(\mathbf{M} - \eta_\gamma\right) \tag{10}$$

In this equation, η_α, η_β, and η_γ are regression parameters. The parameters Q_0, η_α, and η_β for the target region were determined from inversions of the target-region data; we judged that the available data were not adequate to determine η_γ, and therefore that parameter was taken as the Sea22 value (5.1278). A comparison of Q is shown in Figure 8 for both the host region (from Sea22) and the target-region (as determined from the inversions). Because Q is magnitude dependent, values are shown for two magnitudes: 4.5 and 7.5. Figure 8 shows that the magnitude dependence of Q is smaller for the target-region than it is for the host-region ($\frac{\partial \eta}{\partial \tanh M}$ = 0.04 and 0.14 for the target and host regions, respectively). There are enough small magnitude data in the target-region dataset that we think the relatively small host- and target-region differences in Q for small earthquakes are real region-specific differences and not an artifact of limited data. The same cannot be said for the differences in Q for larger earthquakes, however, as data for such events are lacking in the target region. We note that the determination of the anelastic attenuation parameter adjustment $\Delta\gamma$ uses the uncertainties in the Q model parameters determined in the inversions.

The adjustments to F_A and development of the logic-tree branches were determined using the following steps for each period of interest:

- Generate *nsim* random samples of Q_0, η_α, η_β, and η_γ, using the mean values, standard errors, and correlation coefficients of the four parameters for both the Sea22 and INL-region inversions (*nsim* = 1000 in this example). The random samples were obtained using the R function *mvrnorm* (Venables and Ripley, 2002), which accounts for the correlation between the parameters.
- For each random sample of the Q parameters:
    - Simulate PSA for the host- and target-regions. These simulations were performed for **M** = 4.4 to 8.0, with a spacing of 0.1 units, and 21 values of R_{JB} (Joyner-Boore distance), logarithmically spaced from 10 km to 120 km. For the sake of illustration in this article, only a period of 0.1 s was considered, although the procedure applies to all periods. (An exception is for the branch corresponding to the mean value of the $\Delta\gamma$ adjustment, which can be made by using the mean values of the Q parameters, without needing simulations for the large numbers of random samples of the Q parameters.) The simulations were computed using the point-source stochastic model (Boore, 2005) with parameters from the Sea22 inversion of CY14. The R_{JB} distance was converted to R_{RUP} using the equation $R_{RUP} = \sqrt{R_{JB}^2 + Z_{TOR}^2}$, where Z_{TOR} (depth to top of rupture), a function of **M**, came from the CY14 model for strike-slip and normal-slip faulting (their equation (5)). The simulated ground motions for the host region and target regions are PSA_{HOST} and PSA_{TARGET}, respectively. The parameter files used in the simulations are available in the electronic supplement.
    - Compute the simulated adjustments $\Delta\gamma_{SIM}$ to the anelastic attenuation using equation (11):

$$\Delta\gamma_{SIM} = \ln\left(\frac{PSA_{TARGET}}{PSA_{HOST}}\right)\Big/ R_{RUP} \qquad (11)$$

      The result for simulations using the mean values of the Q parameters is plotted in Figure 9a for a period of 0.1 s and magnitudes 4.5 and 7.5. There is some dependence of $\Delta\gamma_{SIM}$ on R_{RUP}, particularly at greater distances. Because distances beyond 100 km are not important to the hazard at INL from crustal

earthquakes, we ignore that dependence, focusing attention on the magnitude dependence. In other applications, however, it might be necessary to include a distance dependence in $\Delta\gamma$.

  - For each magnitude, compute $\overline{\Delta\gamma}$, the average of $\Delta\gamma_{SIM}$ from 30 to 100 km. There will be *nsim* values of $\overline{\Delta\gamma}$ for each magnitude. The values for **M** = 4.5 and 7.5 are shown as the horizontal lines in Figure 9a.

- For each value of **M:**
  - Find the mean and standard deviation of $\overline{\Delta\gamma}$ over all the simulations.
  - Use the 5-point Miller and Rice (1983) procedure to sample the CDF corresponding to a normal distribution defined by the mean and standard deviation in the previous step. These values can be used as the $\Delta\gamma$ adjustments to the CY14 GMPM for the 5 branches of the logic tree. The values for all magnitudes are plotted in Figure 9b for the samples corresponding to the lowest, middle, and highest values of the CDF samples.
- Because of the magnitude dependence of $\Delta\gamma$ shown in Figure 9b, it is convenient for use in applications to fit a polynomial to $\Delta\gamma$ as a function of **M**. For the example given in this article, we found that the following equation was a reasonable fit to $\Delta\gamma$ as a function of **M:**

$$\Delta\gamma = c_0 + c_1(\mathbf{M} - 6) + c_2(\mathbf{M} - 6)^2 + c_3(\mathbf{M} - 6)^3 \quad (12)$$

  This equation gives the adjustment $\Delta\gamma$ to the F_A function given by equation (1e). The coefficients of the polynomial, c_0 through c_3, are provided in Table 2 for the 5 branches of the logic tree, and the fits to **M** are shown in Figure 9b for 3 branches.

The revised function F_A is now given by adding $\Delta\gamma$ from equation (12) to γ in equation (1e):

$$F_A = (\gamma + \Delta\gamma)R_{RUP} \quad (13)$$

A comparison of the host region γ and the adjustment $\Delta\gamma$ is given in Figure 10 as a function of period for four magnitudes for the middle branch of the logic tree (the range for all branches for $T = 0.1$ s is shown by the bars on the value of $\Delta\gamma$ corresponding to that period). Note that there

is less magnitude dependence in $\Delta\gamma$ than in γ. In addition, $\Delta\gamma$ is negative for almost all periods and magnitudes, which means that the ground-motion intensity measures decay more rapidly with distance in the target region than the host region, particularly for short periods.

As mentioned above, the simulations used all of the Sea22 optimal model parameters except for the Q function. One of the parameters needed in the conversion from FAS to PSA is the distance dependence of the duration due to the propagation of waves from the source to the site. Sea22 used the Boore and Thompson (2014) model for the path-component of the durations (the other component being the source duration). It is possible to validate this duration model using the INL-region data, but this was not done in this study.

EPISTEMIC UNCERTAINTY IN THE RESULTING LOGIC TREE

The application of the adjustments for inherent features of the CY14 model that can be viewed as epistemic uncertainties (long-period spectral amplitudes and scaling for normal-faulting earthquakes) and for the two fundamental host-to-target source and site differences (median stress parameter and anelastic attenuation), lead to a logic tree with four nodes and a large number of branch combinations. The logic tree for the nodes and branches discussed in this article is shown in Figure 11. The branches are for $\ln y_{ref}$ (equation (1)). The numbers in the subscripts for the two region-specific adjustments are the branch numbers from the bottom up, and correspond to the weights in Tables 1 and 2.

Recalling the objective of capturing the CBR of TDI, the final stage of completing the GMC logic-tree is to assess whether the branches collectively capture a sufficiently broad range of epistemic uncertainty, and if not, to add nodes and/or branches to broaden the distribution of predicted ground-motion amplitudes. There is no direct way, by definition, to quantify the correct range of epistemic uncertainty, but comparisons can be made to guide and inform the expert judgement. For example, plots can be generated for appropriate ranges of magnitude and distance of the model-to-model variability of the median prediction from the GMC logic-tree, and these can then be compared to similar plots for other suites of GMPMs that might be considered as a lower bound for the range of epistemic uncertainty. An obvious candidate for such a comparative baseline could be the model-to-model variability of the NGA-West2

GMPMs, which might be considered as a lower bound against which the target region epistemic uncertainty could be compared. However, this may not be as straightforward as it sounds, for a number of reasons. Firstly, the model-to-model variability of the NGA-West2 equations is found to diminish with increasing magnitudes, which is counterintuitive since the uncertainty would be expected to increase in the magnitude range where data are sparser. Secondly, the comparison of the GMC logic-tree for the INL-region site with the NGA-West2 models warrants careful consideration, since the latter applies to a much larger region (and indeed combines data from several regions) and the site characterization data available for the NGA-West2 database is generally inferior to the detailed site information gathered for the target locations at INL. Nonetheless, taken at face value, the comparisons suggested that, overall, the level of uncertainty in the INL-region model is equal to or greater than that represented by the NGA-West2 models. However, the true range of epistemic uncertainty in the NGA-West2 models should include the additional intra-model uncertainty proposed by Al Atik and Youngs (2014) (AAY14) in the predictions of the median ground-motion intensity measures (GMIMs), based on the density of the database in different magnitude-distance bins. The AAY14 model for additional epistemic uncertainty could therefore be added as a fifth node to the INL-region logic tree; this would be similar to the epistemic uncertainty branches shown in Figure 10 of AAY14. The AAY14 model includes epistemic uncertainty for strike-slip and reverse ruptures (taken together), as well as for normal-faulting earthquakes. Although the latter model leads to greater increases of epistemic uncertainty, to reflect the relative paucity of recordings from normal-faulting earthquakes in the NGA-West2 database, we suggest using the uncertainties for only the strike-slip and reverse faulting cases, as the deficiency due to the lack of normal faulting data has already been addressed in the INL-region logic-tree through the node for normal-faulting factors.

In assessing the epistemic uncertainty captured by the GMC logic-tree for the INL target region, it is important to bear in mind that it only captures the epistemic uncertainty in the reference rock motions. The reference rock hazard could be convolved with site adjustment factors that are developed to capture the full range of epistemic uncertainty in the site response characteristics (Rodriguez-Marek, Bommer, et al. 2021), in which case the total epistemic uncertainty in the surface hazard at the target horizons would be represented by the combination of the uncertainty in the rock motions and the uncertainty in the site adjustment factors.

DISCUSSION AND CONCLUSIONS

For site-specific PSHA studies, we believe that it would now be difficult to justify the continued approach of building the ground-motion logic-tree by populating the branches with published GMPMs selected and weighted on the basis of their potential applicability to the target region. A superior approach is to select a backbone GMPM, chosen for being amenable to host-to-target region adjustments rather than any inherent applicability to the target region, and to then construct the logic-tree as a series of nodes for the individual adjustments for host-to-target region differences in source and path parameters. We recognize that the method described in this article would be a challenge to apply either for hazard analyses over broad regions or for sites with very limited data on which to base host-to-target adjustments.

This paper has built on the work of Bommer and Stafford (2020) in which CY14 was identified as the most suitable of all current GMPMs for shallow crustal earthquakes in terms of its adaptability through individual adjustments for host-to-target region differences in source (stress parameter, $\Delta\sigma$) and path (anelastic attenuation quality factor, Q) characteristics. Subsequent work by Al Atik and Abrahamson (2021) provided a V_S profile and κ_0 consistent with rock ($V_{S30} = 760$ m/s) predictions from CY14, which Stafford et al. (2022) used to invert the CY14 for model-consistent estimates of the stress parameter $\Delta\sigma$ and the attenuation quality factor Q. In this study, these host-region characteristics have been used as the starting point for the construction of a logic-tree for ground-motion predictions in reference rock for the Idaho National Laboratory, using target-region estimates of $\Delta\sigma$ and Q obtained from analysis of local and regional ground-motion recordings. The logic-tree also includes nodes for adjustments that address the lack of constraint for normal-faulting earthquakes in the CY14 database and the unique treatment of long-period spectral ordinates in the derivation of that model. Additionally, for the INL study it was decided to include an additional node to impose the additional epistemic uncertainty proposed by Al Atik and Youngs (2014) for the NGA-West2 models, given that this should be applied in the host region and therefore cannot be omitted from the target region.

In the future, we expect new GMPMs to be published that are as suitable for host-to-target adjustments as the CY14 model, and possibly superior in other regards such as including better constraints on normal-faulting earthquake ground motions. Until such time, however, the

procedure illustrated herein could be applied to any site-specific PSHA in regions of shallow crustal seismicity, which could significantly simplify the construction of the ground-motion logic-tree for reference rock motions. Adopting this framework, with CY14 as the backbone GMPM, the host-region characteristics are now readily available and the methodology for making host-to-target region adjustments have been explained. The ground-motion model-building component of any site-specific PSHA project can therefore focus almost exclusively on the estimation of target-region source and path parameters, and then on the adjustment from reference rock profile of CY14 to the target site profile.

DATA AND RESOURCES

The site-amplification-adjusted, logarithmically smoothed, vector-summed FAS used in the inversions are included in the supplemental materials. The figures were prepared using CoPlot (www.cohortsoftware.com, last accessed July 2022). The simulations needed for the F_S and F_A adjustments were computed using *tmrsk_loop_rv_drvr*, and *tmrsk_loop_rv_drvr_for_random_samples_of_Sea22_Q_params*, programs included in the SMSIM suite of programs (Boore, 2005), available from the online software link on http://www.daveboore.com (last accessed July 2022). Most of the analysis used scripts written in the statistical language and environment R (R Core Team, 2022) (https://www.R-project.org/, last accessed July 2022). Inversions were performed using *pymc3* (Salvatier et al., 2016). Supplemental Material for this article includes the site-amplification-adjusted Fourier acceleration spectra used in this study for the INL region and the parameter and control files used in the simulations.

DECLARATION OF COMPETING INTERESTS

The authors acknowledge that there are no conflicts of interest recorded.

ACKNOWLEDGMENTS

We thank Carola Di Alessandro, John Douglas, and an anonymous reviewer for useful reviews.

REFERENCES

Abrahamson, N. A., W. J. Silva, and R. Kamai (2014). Summary of the ASK14 ground motion relation for active crustal regions, *Earthquake Spectra* **30**, 1025–1055.

Ake, J., C. Munson, J. Stamatakos, M. Juckett, K. Coppersmith, and J. Bommer (2018). Updated Implementation Guidelines for SSHAC Hazard Studies, U. S. Nuclear Regulatory Commission, NUREG-2213, 145 pp.

Akkar, S., M. A. Sandıkkaya, and J. J. Bommer (2014a). Empirical ground-motion models for point- and extended-source crustal earthquake scenarios in Europe and the Middle East. *Bull. of Earthquake Engineering* **12**, 359–387.

Akkar, S., M. A. Sandıkkaya, and J. J. Bommer (2014b). Erratum to: Empirical ground-motion models for point- and extended-source crustal earthquake scenarios in Europe and the Middle East, *Bull. of Earthquake Engineering* **12**, 389–390.

Al Atik, L., and N. Abrahamson (2021). A methodology for the development of 1D reference V_S profiles compatible with ground-motion prediction equations: Application to NGA-West2 GMPEs, *Bull. Seismol. Soc. Am.* **111**, 1765–1783.

Al Atik, L., and R. R. Youngs (2014). Epistemic uncertainty for NGA-West2 models. *Earthquake Spectra* **30**, 1301–1318.

Ancheta, T. D., R. B. Darragh, J. P. Stewart, E. Seyhan, W. J. Silva, B. S. J. Chiou, K. E. Wooddell, R. W. Graves, A. R. Kottke, D. M. Boore, T. Kishida, and J. L. Donahue (2014). NGA-West2 database, *Earthquake Spectra* **30**, 989–1005.

Atkinson, G. M., J. J. Bommer, and N. A. Abrahamson (2014). Alternative approaches to modeling epistemic uncertainty in ground motions in probabilistic seismic-hazard analysis. *Seismological Research Letters* **85**, 1141–1144.

Bazzurro, P., and C. A. Cornell (2004). Nonlinear soil-site effects in probabilistic seismic-hazard analysis, *Bull. Seismol. Soc. Am*. **94**, 2110–2123.

Bindi, D., M. Massa, L. Luzi, G. Ameri, F. Pacor, R. Puglia, and P. Augliera (2014a). Pan-European ground-motion prediction equations for the average horizontal component of PGA, PGV, and 5%-damped PSA at spectral periods up to 3.0 s using the RESORCE dataset, *Bull. of Earthquake Engineering* **12**, 391–430.

Bindi, D., M. Massa, L. Luzi, G. Ameri, F. Pacor, R. Puglia, and P. Augliera (2014b). Erratum to: Pan-European ground-motion prediction equations for the average horizontal component of PGA, PGV, and 5%-damped PSA at spectral periods up to 3.0 s using the RESORCE dataset, *Bull. of Earthquake Engineering* **12**, 431–448.

Bommer, J. J. (2012). Challenges of building logic trees for probabilistic seismic hazard analysis, *Earthquake Spectra*, **28**, 1723–1735.

Bommer, J. J., and F. Scherbaum (2008). The use and misuse of logic trees in probabilistic seismic hazard analysis, *Earthquake Spectra*, **24**, 997–1009.

Bommer, J. J., and P. J. Stafford (2020). Selecting ground-motion models for site-specific PSHA: adaptability versus applicability, *Bull. Seismol. Soc. Am.* **110**, 2801–2815, doi: 10.1785/0120200171

Boore, D.M. (1983). Stochastic simulation of high-frequency ground motions based on seismological models of the radiated spectra, *Bull. Seismol. Soc. Am.* **73**, 1865–1894.

Boore, D. M. (2003). Simulation of ground motion using the stochastic method. *Pure and Applied Geophysics* **160**, 635–676.

Boore, D. M. (2005). SMSIM---Fortran Programs for Simulating Ground Motions from Earthquakes: Version 2.3---A Revision of OFR 96-80-A, U.S. Geological Survey Open-File Report, *U. S. Geological Survey Open-File Report* **00-509**, revised 15 August 2005, 55 pp.

Boore, D. M., and E. M. Thompson (2014). Path durations for use in the stochastic-method simulation of ground motions, *Bull. Seismol. Soc. Am.* **104**, 2541–2552. doi: 10.1785/0120140058

Boore, D. M., J. P. Stewart, E. Seyhan, and G. M. Atkinson (2014). NGA-West 2 equations for predicting PGA, PGV, and 5%-Damped PSA for shallow crustal earthquakes, *Earthquake Spectra* **30**, 1057–1085.

Boore, D. M., J. P. Stewart, A. Skarlatoudis, E. Seyhan, B. Margaris, N. Theodoulidis, E. Scordilis, I. Kalogeras, N. Klimis, and N. S. Melis (2020). A ground-motion prediction model for shallow crustal earthquakes in Greece, *Bull. Seismol. Soc. Am.* **111**, 857–874.

Campbell, K. W. (2003). Prediction of strong ground motion using the hybrid empirical method and its use in the development of ground-motion (attenuation) relations in eastern North America, *Bull. Seismol. Soc. Am*. **93**, 1012–1033.

Campbell, K. W., and Y. Bozorgnia (2014). NGA-West2 ground motion model for the average horizontal components of PGA, PGV, and 5% damped linear acceleration response spectra, *Earthquake Spectra* **30**, 1087–1115.

Chiou, B. S. J., and R. R. Youngs (2008). NGA Model for Average Horizontal Component of Peak Ground Motion and Response Spectra, *PEER Report 2008/09*, Pacific Earthquake Engineering Research Center, University of California, Berkeley, 293 pp.

Chiou, B. S. J., and R. R. Youngs (2014). Update of the Chiou and Youngs NGA Model for the Average Horizontal Component of Peak Ground Motion and Response Spectra, *Earthquake. Spectra* **30**, 1117–1153.

Chiou, B. S. J., R. Darragh, N. Gregor, and W. Silva (2008). NGA project strong-motion database, *Earthquake Spectra* **24**, 23–44.

Goulet, C., Y. Bozorgnia, N. Abrahamson, N. Kuehn, L. Al Atik, R. Youngs, R. Graves, and G. Atkinson (2018). Central and Eastern North America Ground-Motion Characterization: NGA-East Final Report, *PEER Report 2018/08*, Pacific Earthquake Engineering Research Center, 817 pp.

Hanks, T. C., and H. Kanamori (1979). A moment magnitude scale, *J. Geophys. Res.* **84**, 2348–2350.

McGuire, R. K., W. J. Silva, and C. J. Costantino (2001). *Technical basis for revision of regulatory guidance on design ground motions: Hazard-and risk-consistent ground motion spectra guidelines*. NUREG/CR-6728, US Nuclear Regulatory Commission, Washington DC.

Miller III, A. C., and T. R. Rice (1983). Discrete approximations of probability distributions. *Management Science* **29**, 352–362.

R Core Team (2022). R: A language and environment for statistical computing. R Foundation for Statistical Computing, Vienna, Austria.

Rodriguez-Marek, A., J. Ake, C. Munson, E. Rathje, S. Stovall, T. Weaver, K. Ulmer, and M. Juckett (2021). *Documentation report for SSHAC Level 2: Site response*. Center for Nuclear Waste Regulatory Analysis, San Antonio, TX. https://www.nrc.gov/docs/ML2132/ML21323A056.pdf

Rodriguez-Marek, A., J. J. Bommer, R. R. Youngs, M. J. Crespo, P. J. Stafford, and M. Bahrampouri (2021). Capturing epistemic uncertainty in site response, *Earthquake Spectra* **37**, 921–936.

Rodriguez-Marek, A., E. M. Rathje, J. J. Bommer, F. Scherbaum, and P. J. Stafford (2014). Application of single-station sigma and site-response characterization in a probabilistic seismic-hazard analysis for a new nuclear site, *Bull. Seismol. Soc. Am.* **104**, 1601–1619.

Salvatier, J., T. V. Wiecki, and C. Fonnesbeck (2016). Probabilistic programming in Python using PyMC3, *PeerJ Computer Science* **2**, e55.

Scherbaum, F., F. Cotton, and H. Staedtke (2006). The estimation of minimum-misfit stochastic models from empirical ground-motion prediction equations, *Bull. Seismol. Soc. Am.* **96**, 427–445.

Scherbaum, F., N. M. Kuehn, M. Ohrnberger, and K. Koehler (2010). Exploring the Proximity of Ground-Motion Models Using High-Dimensional Visualization Techniques, *Earthquake Spectra* **26**, 1117–1138.

Silva, W., B. Darragh, T. Kishida, O.-J. Ktenidou, and E.-V. Pikoulis (2021). INL SSHAC Level 3 study: Estimation of source, path, and site parameters and their uncertainty, *INL Report INL/EXT-21-65281,* Idaho National Laboratory, Idaho Falls, 259 pp.

Skarlatoudis, A. A., C. B. Papazachos, B. N. Margaris, N. Theodulidis, Ch. Papaioannou, I. Kalogeras, E. M. Scordilis, and V. Karakostas (2003). Empirical peak ground-motion predictive relations for shallow earthquakes in Greece, *Bull. Seismol. Soc. Am.* **93**, 2591–2603.

Spudich, P., and D. M. Boore (2005). ERRATUM: Bulletin of the Seismological Society of America, Vol. 89, No. 5, pp. 1156-1170, October 1999, SEA99: A Revised Ground Motion Prediction Relation for Use in Extensional Tectonic Regimes, by P. Spudich, W. B. Joyner, A. G. Lindh, D. M. Boore, B. M. Margaris, and J. B. Fletcher, *Bull. Seismol. Soc. Am.* **95**, 1209.

Spudich, P., J. B. Fletcher, M. Hellweg, J. Boatwright, C. Sullivan, W. B. Joyner, T. C. Hanks, D. M. Boore, A. McGarr, L. M. Baker, and A. G. Lindh (1996). Earthquake ground motions in extensional tectonic regimes, *U.S. Geological Survey Open-File Report* **96-292**, 351 pp.

Spudich, P., W. B. Joyner, A. G. Lindh, D. M. Boore, B. M. Margaris, and J. B. Fletcher (1999). SEA99: A revised ground motion prediction relation for use in extensional tectonic regimes, *Bull. Seismol. Soc. Am.* **89**, 1156–1170.

Stafford, P. J., D. M. Boore, R. R. Youngs, and J. J. Bommer (2022). Host-region parameters for an adjustable model for crustal earthquakes to facilitate the implementation of the backbone approach to building ground-motion logic trees in probabilistic seismic hazard analysis, *Earthquake Spectra* **38**, 917–949.

USNRC (2018). *Updated implementation guidelines for SSHAC hazard studies*. NUREG-2213, US Nuclear Regulatory Commission, Washington DC.

Venables, W. N., and B. D. Ripley (2002). *Modern Applied Statistics with S*, Fourth edition, Springer, New York, 495 pp.

AUTHOR AFFILIATIONS

David M. Boore*[1], Robert R. Youngs[2], Albert R. Kottke[3], Julian J. Bommer[4], Robert Darragh[5], Walter J. Silva[5], Peter J. Stafford[4], Linda Al Atik[6], Adrian Rodriguez-Marek[7], and James Kaklamanos[8]

1. Consultant, Los Altos, CA, USA
2. Wood Environment & Infrastructure Solutions, Inc., Oakland, CA, USA
3. Pacific Gas & Electric Company, San Francisco, CA, USA
4. Dept. of Civil and Environmental Engineering, Imperial College London, London SW7 2AZ, UK
5. Pacific Engineering & Analysis, El Cerrito, CA 94530, USA
6. Al Atik Consulting, San Francisco, CA, USA
7. Department of Civil and Environmental Engineering, Virginia Tech, Blacksburg, VA, USA
8. Department of Civil Engineering, Merrimack College, North Andover, MA, USA

*Corresponding author: dboore@yahoo.com

FIGURE CAPTIONS

Figure 1. 5%-damped PSA as a function of period for four NGA-West2 GMPMs, for the predictor variables shown in the legend (SS = strike-slip, FW = footwall). ASK14 = Abrahamson et al. (2014), BSSA14 = Boore et al. (2014), CB14 = Campbell and Bozorgnia (2014), CY14 = Chiou and Youngs (2014).

Figure 2. a) Ratio of the geometric mean of PSA from ASK14, BSSA14, and CB14 to the PSA from CY14; b) the Δc_1 adjustments to F_C.

Figure 3. a) Ratios of PSA for normal-slip and strike-slip earthquakes for a number of GMPMs. Aea14a,b = Akkar et al. (2014a, b), Bea14a,b = Bindi et al. (2014a,b); the other acronyms are defined in the caption to Figure 1. b) the CY14 style-of-faulting (SoF) adjustment as modified by the additional term given by α_{NM}, for two magnitudes.

Figure 4. The magnitude-distance distribution of earthquakes in the target region around the Idaho National Laboratory (INL) used in the inversion to obtain parameters for the target region.

Figure 5. Stress parameters obtained by inverting the Fourier acceleration records from the target region. The lines are from a variance-weighted fit to the function in equation (7). The values of $\Delta\sigma_{\mathbf{M5}}$ for the lowest, middle, and highest logic-tree branches are also shown for comparison.

Figure 6. The cumulative distribution function (CDF) of $\Delta\sigma_{\mathbf{M5}} = \Delta\sigma(\mathbf{M} = 5)$ from the host region (CY14) and from inversions of the simulated target-region stress-parameter data (see text). The $\Delta\sigma_{\mathbf{M5}}$ for the Miller and Rice (1983) 5-point approximation (vertical dashed lines) are shown for the target region only.

Figure 7. The target-region source function F_S for the lowest, middle, and highest logic-tree branches. The adjusted hinge magnitude is shown for each branch, where Δc_M is calculated from the $\Delta\sigma_{\mathbf{M5}}$ for each branch. For comparison, also shown is F_S for the host region (CY14).

Figure 8. The Q attenuation parameter using the mean Q_0, η_α, η_β, and η_γ from the Sea22 inversion of CY14 and from the regression analysis of the target-region data.

Figure 9. a) the anelastic attenuation parameter $\Delta\gamma_{SIM}$ computed from the logarithm of the ratio of simulated PSA using mean parameters for the target region and for the CY14 GMPM for one period (0.1 s) and two magnitudes (4.5 and 7.5). The short horizontal lines are averages of $\Delta\gamma$ from 30 to 100 km ($\overline{\Delta\gamma}$). b) $\overline{\Delta\gamma}$ vs. **M** for T = 0.1 s for the lowest, middle, and highest logic-tree branches (see Table 2). The two values for **M** = 4.5 and **M** = 7.5 plotted using larger symbols correspond to the short horizontal lines in graph a).

Figure 10. The anelastic attenuation (F_A) parameter γ from CY14, and the adjustment $\Delta\gamma$ developed in this article for the middle logic-tree branch (the mean value of $\Delta\gamma$, which was developed using the mean values of the Q parameters, without the need for multiple simulations). The results of using the 1000 simulations are shown by the symbols for $\Delta\gamma$ at T = 0.1 s, with the bars for $\Delta\gamma$ at T = 0.1 s corresponding to the lowest and highest logic-tree branches. The target-region attenuation parameter is given by $\gamma + \Delta\gamma$.

Figure 11. The complete logic tree for the four adjustments discussed in this article. The numbered subscripts for the source and anelastic attenuation branches correspond to the logic-tree branch numbers, with parameter values given in Tables 1 and 2. The weights are given in parentheses below each branch.

Figure A1. Illustration of the dependence of the magnitude scaling on the stress parameter $\Delta\sigma$ (see text for discussion of the various parts of the figure). As a side note, the *FS* in parts a) and c) rises slowly at high frequencies rather than being flat, as implied by equation (A5), because the Al Atik and Abrahamson (2021) crustal amplifications, which increase with frequency, have been included (and $\kappa_0 = 0$ s, so the *FS* at high frequencies is not reduced).

Figure A2. Illustrating the scaling of Fourier spectra (*FS*) and response spectra (*RS*) for negative (left side) and positive (right side) shifts in $\Delta c_{M,FS}$, showing that the shift in $\Delta c_{M,RS}$ needs to be modified from that for $\Delta c_{M,FS}$ in order for the *RS* amplitude of line-segment 2 to be similar to that of the *FS* line-segment 2 amplitude.

TABLES

Table 1. Information related to the logic-tree branches for the F_S host-to-target adjustment to the CY14 GMPM for an oscillator period of 0.1 s. The units of $\Delta\sigma$ are bars. The branches are numbered from the smallest to the largest values of the Δc_M adjustment.

T(s)	branch	CDF	$\Delta\sigma_{Host}$	$\Delta\sigma_{Target}$	Δc_M	weight
0.1	5	0.96511	105.1	131.4	0.183	0.101
0.1	4	0.78830	101.9	103.8	0.015	0.244
0.1	3	0.50000	99.4	86.1	-0.110	0.309
0.1	2	0.21170	96.9	71.4	-0.234	0.244
0.1	1	0.03489	94.0	56.4	-0.391	0.101

Table 2. Logic-tree branches for F_A. The last four columns are coefficients of equation (12) giving $\Delta\gamma$ as a function of **M** for the various branches. The branches are numbered from the smallest to the largest values of the $\Delta\gamma$ adjustment. Although the results are for a single period (0.1 s), the procedure can be used without alteration to obtain the values in the table for any period.

T (s)	branch	CDF	weight	c_0	c_1	c_2	c_3
0.1	5	0.96511	0.101	-6.018E-03	-2.559E-04	2.264E-04	-5.598E-05
0.1	4	0.78830	0.244	-6.236E-03	-2.735E-04	2.197E-04	-5.195E-05
0.1	3	0.50000	0.309	-6.409E-03	-2.874E-04	2.144E-04	-4.877E-05
0.1	2	0.21170	0.244	-6.582E-03	-3.013E-04	2.091E-04	-4.558E-05
0.1	1	0.03489	0.101	-6.800E-03	-3.189E-04	2.024E-04	-4.155E-05

FIGURES

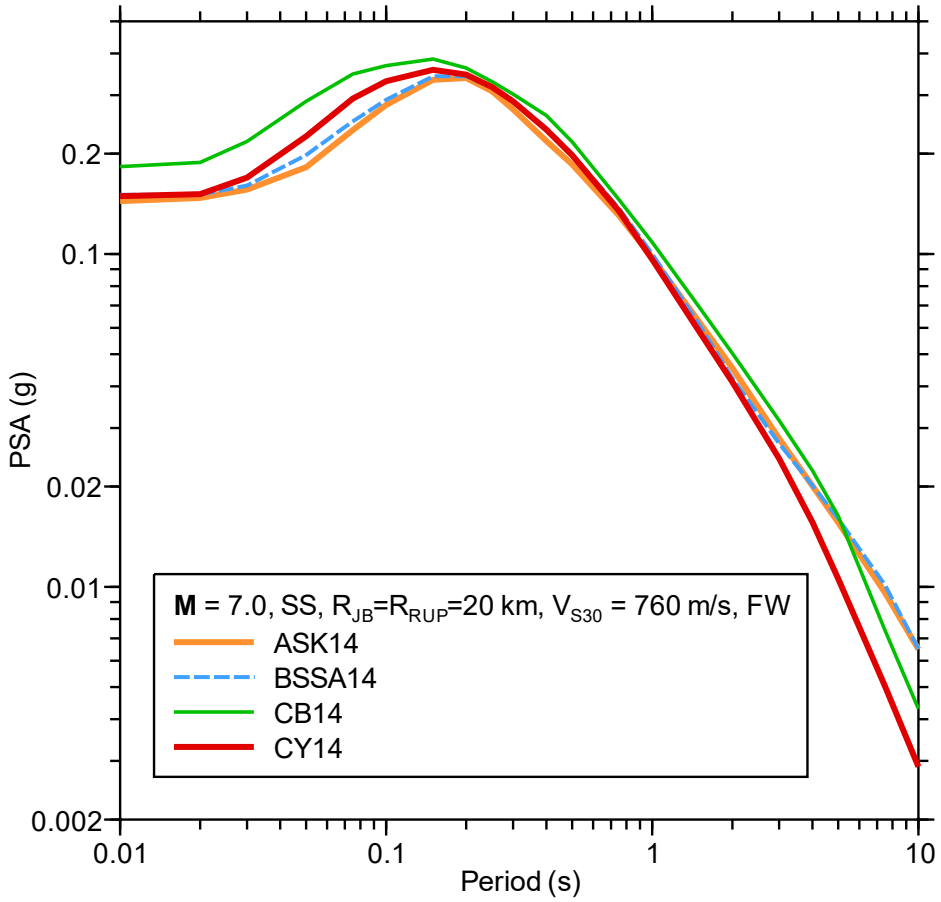

Figure 1. 5%-damped PSA as a function of period for four NGA-West2 GMPMs, for the predictor variables shown in the legend (SS = strike-slip, FW = footwall). ASK14 = Abrahamson et al. (2014), BSSA14 = Boore et al. (2014), CB14 = Campbell and Bozorgnia (2014), CY14 = Chiou and Youngs (2014).

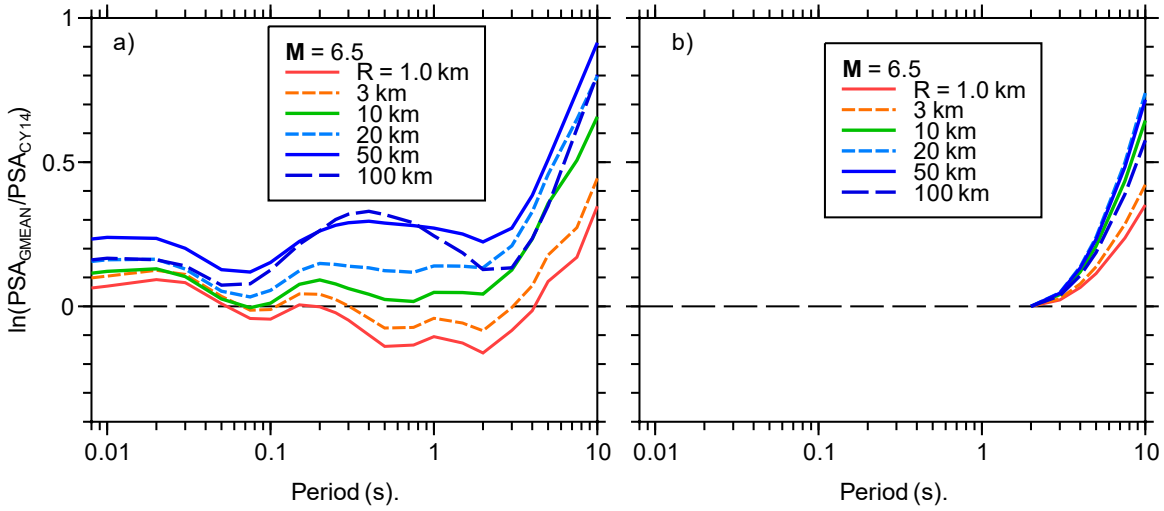

Figure 2. a) Ratio of the geometric mean of PSA from ASK14, BSSA14, and CB14 to the PSA from CY14; b) the Δc_1 adjustments to F_C.

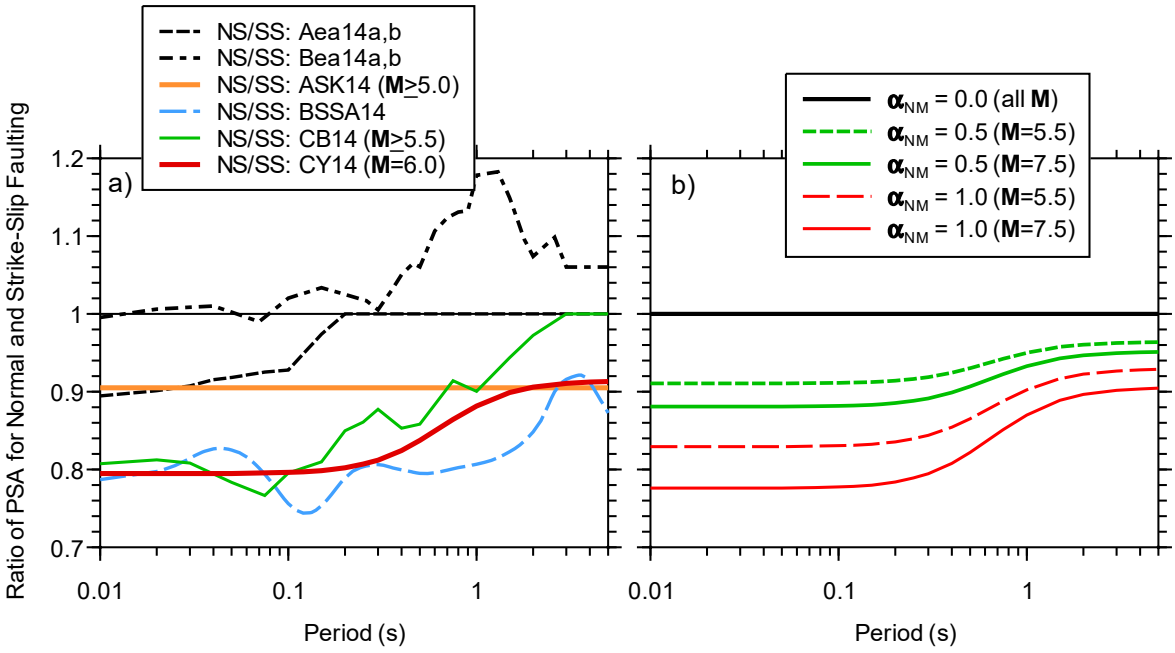

Figure 3. a) Ratios of PSA for normal-slip and strike-slip earthquakes for a number of GMPMs. Aea14a,b = Akkar et al. (2014a, b), Bea14a,b = Bindi et al. (2014a,b); the other acronyms are defined in the caption to Figure 1. b) the CY14 style-of-faulting (SoF) adjustment as modified by the additional term given by α_{NM}, for two magnitudes.

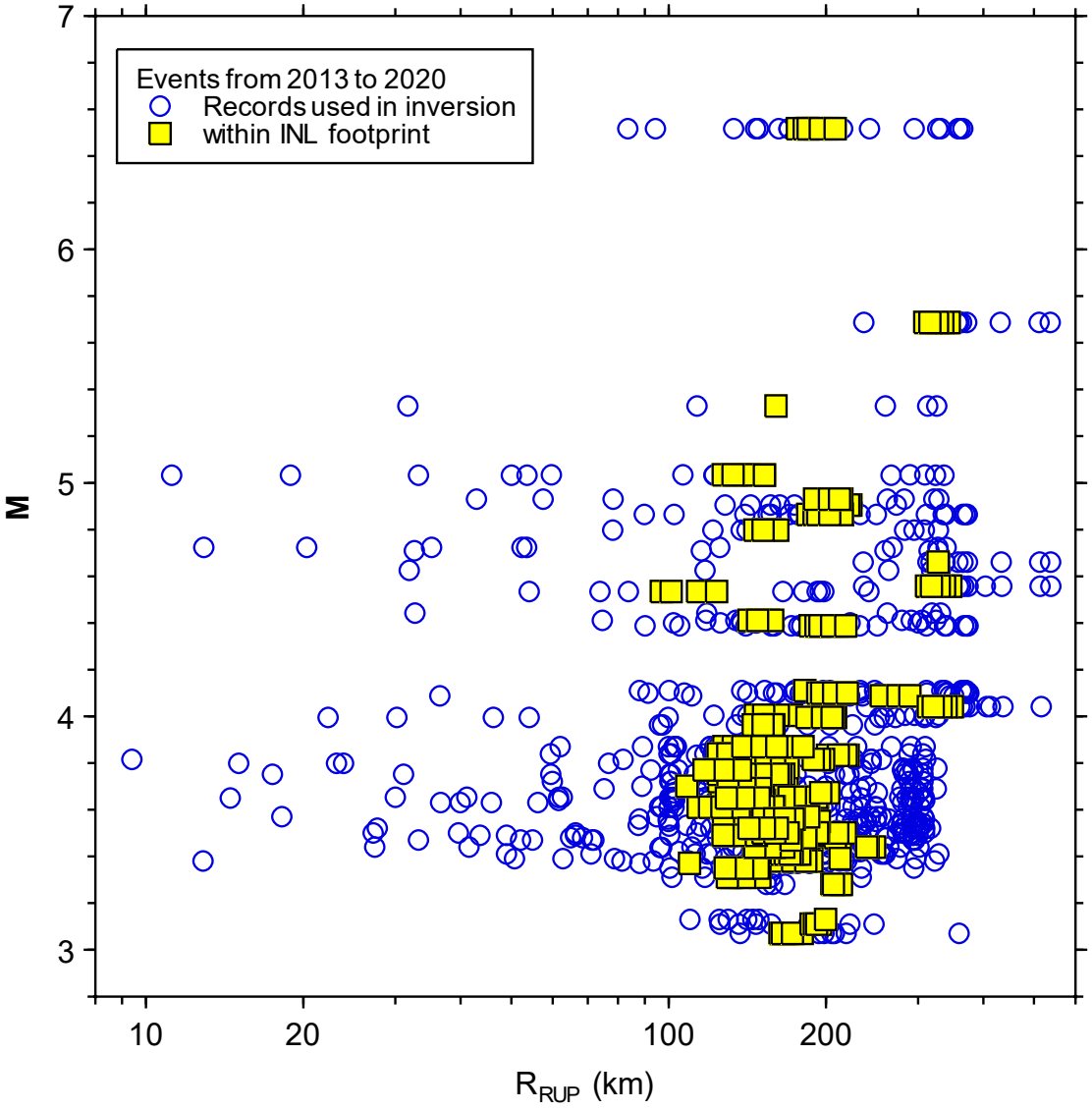

Figure 4. The magnitude-distance distribution of earthquakes in the target region around the Idaho National Laboratory (INL) used in the inversion to obtain parameters for the target region.

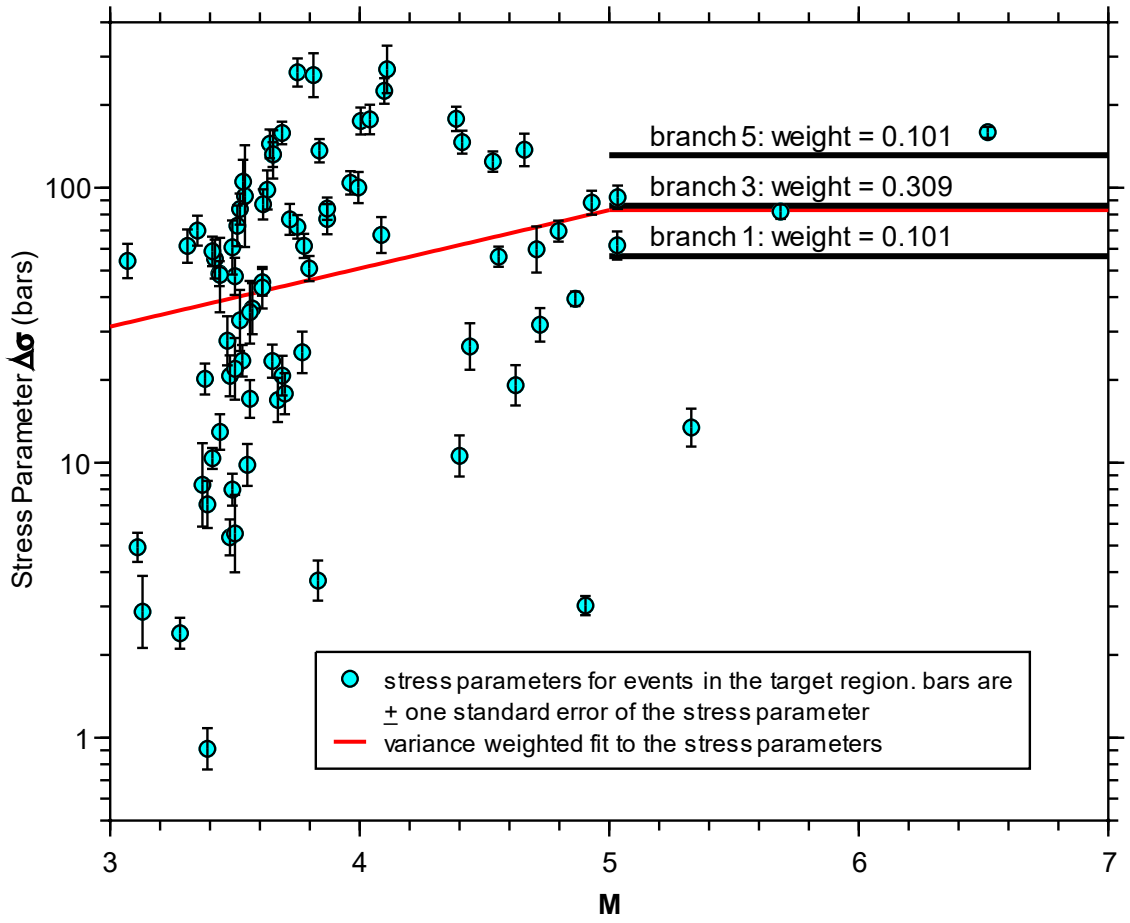

Figure 5. Stress parameters obtained by inverting the Fourier acceleration records from the target region. The lines are from a variance-weighted fit to the function in equation (7). The values of $\Delta\sigma_{\mathbf{M5}}$ for the lowest, middle, and highest logic-tree branches are also shown for comparison.

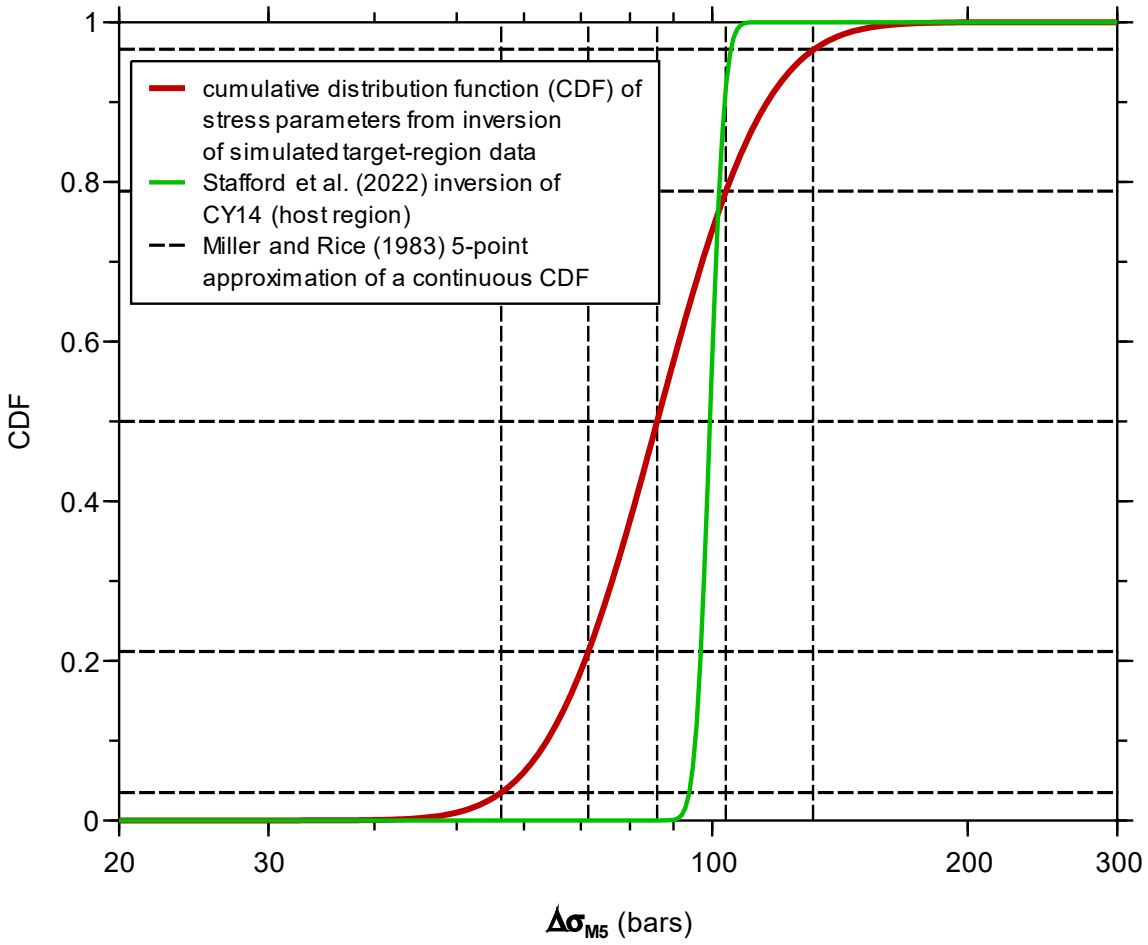

Figure 6. The cumulative distribution function (CDF) of $\Delta\sigma_{\mathbf{M5}} = \Delta\sigma(\mathbf{M} = 5)$ from the host region (CY14) and from inversions of the simulated target-region stress-parameter data (see text). The $\Delta\sigma_{\mathbf{M5}}$ for the Miller and Rice (1983) 5-point approximation (vertical dashed lines) are shown for the target region only.

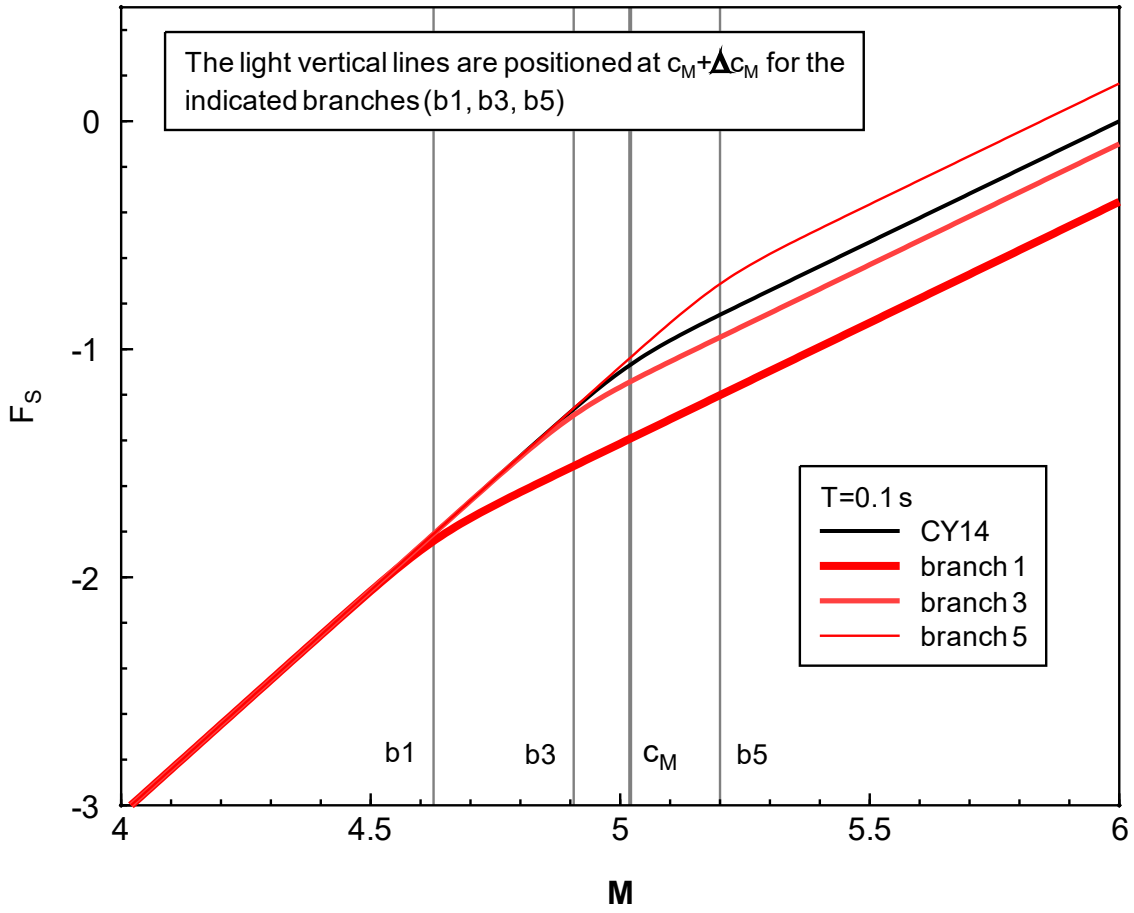

Figure 7. The target-region source function F_S for the lowest, middle, and highest logic-tree branches. The adjusted hinge magnitude is shown for each branch, where Δc_M is calculated from the $\Delta\sigma_{\mathbf{M5}}$ for each branch. For comparison, also shown is F_S for the host region (CY14).

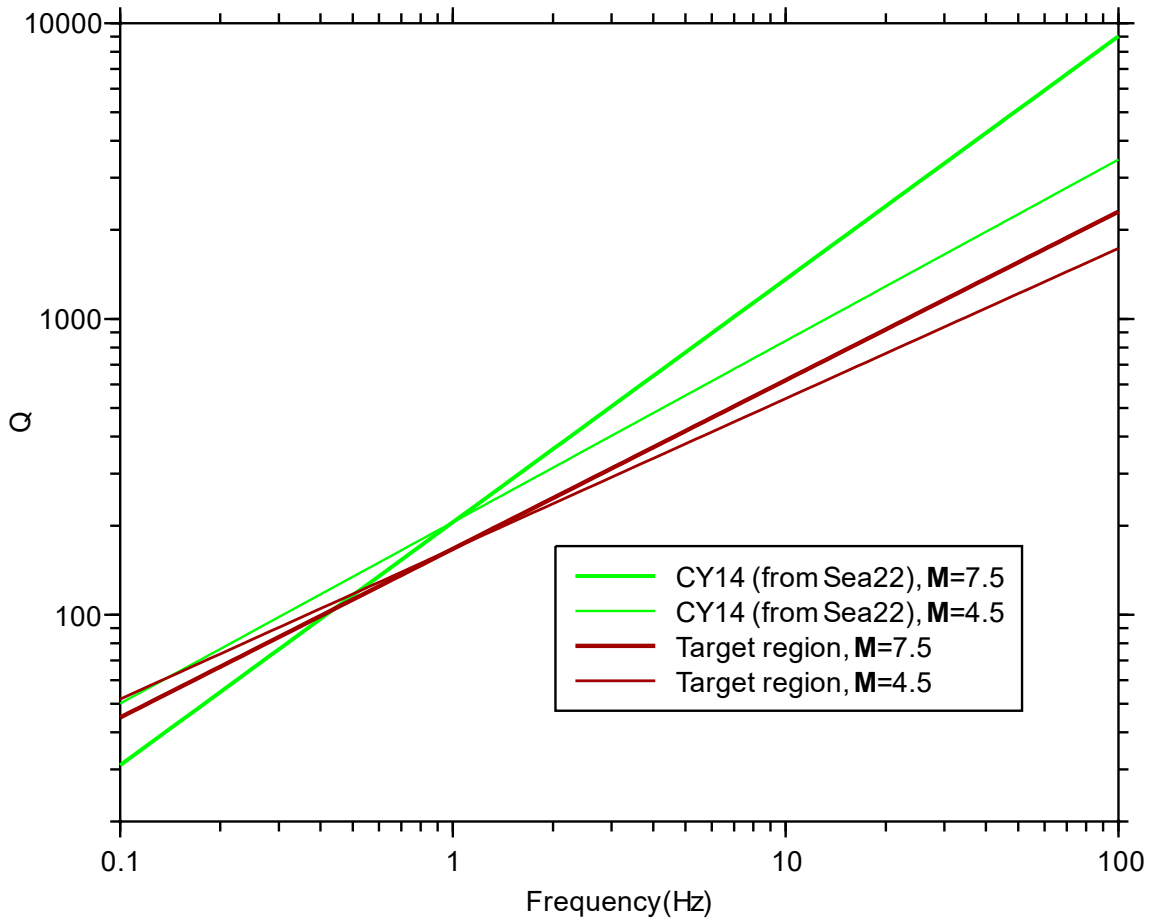

Figure 8. The Q attenuation parameter using the mean Q_0, η_α, η_β, and η_γ from the Sea22 inversion of CY14 and from the regression analysis of the target-region data.

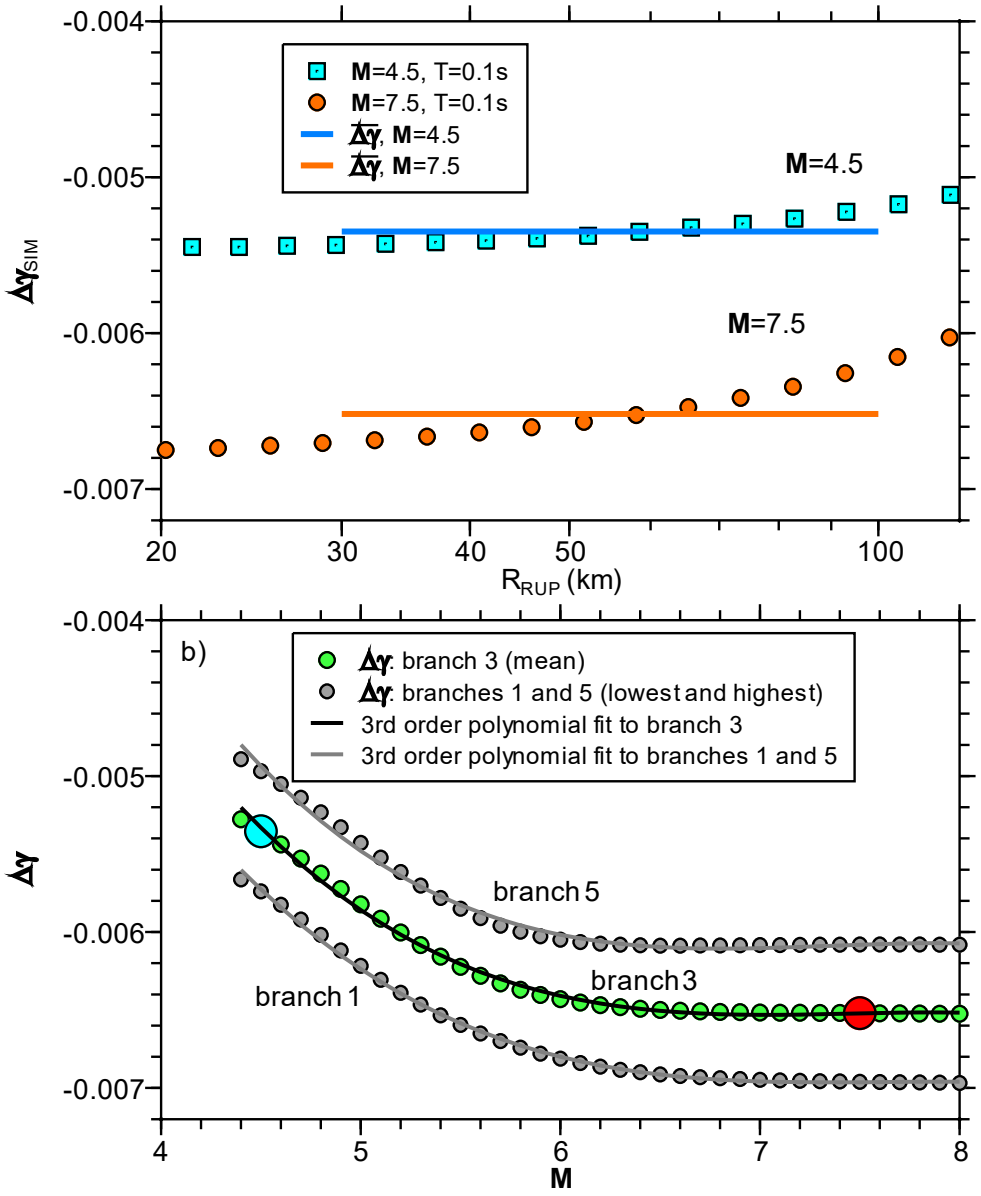

Figure 9. a) the anelastic attenuation parameter $\Delta\gamma_{SIM}$ computed from the logarithm of the ratio of simulated PSA using mean parameters for the target region and for the CY14 GMPM for one period (0.1 s) and two magnitudes (4.5 and 7.5). The short horizontal lines are averages of $\Delta\gamma$ from 30 to 100 km ($\overline{\Delta\gamma}$). b) $\overline{\Delta\gamma}$ vs. **M** for T = 0.1 s for the lowest, middle, and highest logic-tree branches (see Table 2). The two values for **M** = 4.5 and **M** = 7.5 plotted using larger symbols correspond to the short horizontal lines in graph a).

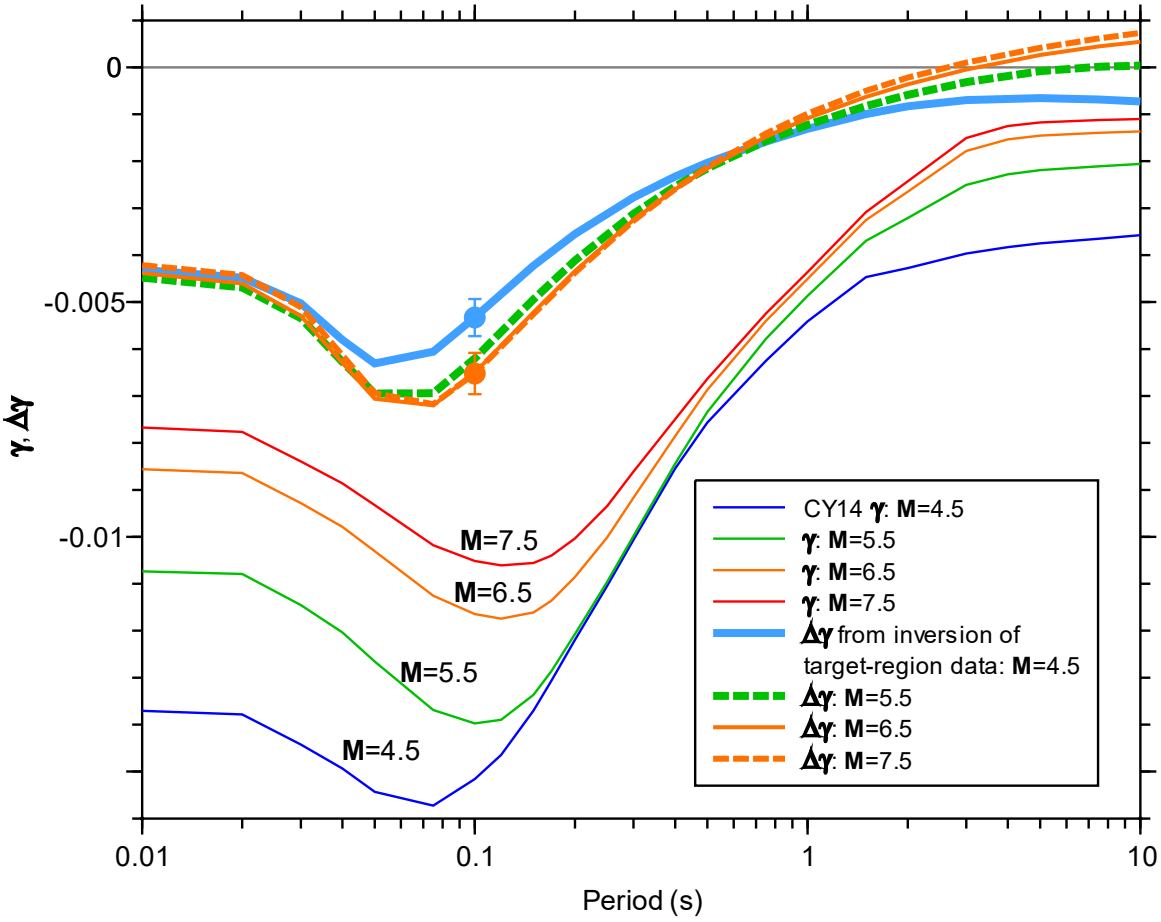

Figure 10. The anelastic attenuation (F_A) parameter γ from CY14, and the adjustment $\Delta\gamma$ developed in this article for the middle logic-tree branch (the mean value of $\Delta\gamma$, which was developed using the mean values of the Q parameters, without the need for multiple simulations). The results of using the 1000 simulations are shown by the symbols for $\Delta\gamma$ at T = 0.1 s, with the bars for $\Delta\gamma$ at T = 0.1 s corresponding to the lowest and highest logic-tree branches. The target-region attenuation parameter is given by $\gamma + \Delta\gamma$.

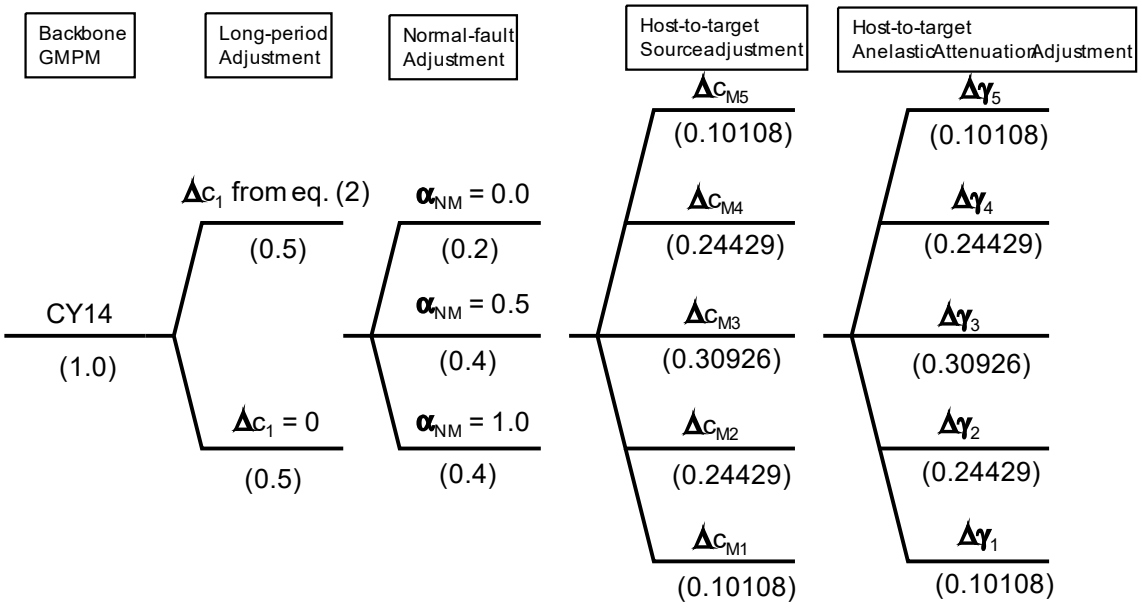

Figure 11. The complete logic tree for the four adjustments discussed in this article. The numbered subscripts for the source and anelastic attenuation branches correspond to the logic-tree branch numbers, with parameter values given in Tables 1 and 2. The weights are given in parentheses below each branch.

APPENDIX. ADJUSTING THE CY14 SOURCE SCALING FOR CHANGES IN THE STRESS PARAMETER

Bommer and Stafford (2020, top left column of p. 2811) suggested that changes in stress parameters can be accounted for by differences in c_M in the CY14 source scaling, but they gave no details. This Appendix provides those details.

The source scaling F_S in CY14 is given primarily by equation (1c), repeated here for convenience:

$$F_S = c_2(\mathbf{M} - 6) + \frac{c_2 - c_3}{c_n}\ln\left[1 + e^{c_n(c_M - \mathbf{M})}\right] \quad \text{(A1)}$$

We say "primarily", because there is also **M** dependence of $\ln y_{ref}$ in the F_{SoF}, F_{Ztor}, F_{Dip}, F_{GS}, and F_A functions. But those functions are not expected to depend on the source scaling as controlled by the stress parameter $\Delta\sigma$. Although it is a continuous, smoothly varying function, the F_S can be thought of as being constructed from two essentially linear segments joined by a short transition segment (an example is shown in Figure 7). The intersection of the two linear segments occurs at $\mathbf{M} = c_M$. We refer to the essentially linear segments as segment 1, for which the **M** scaling is determined by the source function at frequencies less than the source corner frequency, and is therefore independent of the stress parameter, and segment 2, whose magnitude scaling is influenced by the stress parameter. Because of the relation of the magnitude scaling to the source spectra, the slope of segment 1 is greater than that of segment 2.

To understand how to change the CY14 source scaling to account for differences in $\Delta\sigma$ it is useful to consider a plot of the Fourier acceleration spectra (*FS*) from a single-corner-frequency, constant stress parameter source, for a suite of moment magnitudes **M**. Such a plot is shown in Figure A1a for $R_{JB} = 10$ km, **M** ranging from 4 to 8 in increments of 0.5, and $\Delta\sigma = 100$ bars. To see the scaling of *FS* with **M**, we plotted *FS* vs **M** in Figure A1b for a frequency of 0.5 Hz (this frequency is shown by the vertical line in Figure A1a). The straight lines in Figure A1b were obtained by fitting lines to the small and large **M** portions of the *FS*. The magnitude scaling

for *FS* is similar to that for response spectra (*RS*) for the CY14 GMPM (e.g., Figure 7), with line segments for small and large **M** intersecting at a hinge magnitude. (For the sake of brevity in the notation, we use *FS* and *RS* for Fourier acceleration spectra and pseudo-acceleration response spectra in this Appendix, rather than FAS and PSA as in the main body of the article). Because of the similarity to the CY14 magnitude scaling, we call the hinge magnitude c_M. The following analysis first derives a relation, based on a model of the scaling of *FS*, giving the change in c_M due to changing the stress parameter from $\Delta\sigma_1$ to $\Delta\sigma_2$. An adjustment is then derived to account for differences in the magnitude-scaling slopes of *FS* and *RS*. We added *FS* and *RS* as subscripts to c_M to differentiate between the hinge magnitudes for *FS* and *RS* when necessary. For simplicity of notation, however, we did not add an additional subscript to c_M in most of the first section, which deals only with *FS*.

CHANGES IN THE HINGE MAGNITUDE FOR FOURIER SPECTRA DUE TO CHANGES IN THE STRESS PARAMETER

To see the effect of a change in $\Delta\sigma$, the *FS* for $\Delta\sigma = 50$ bars has been added to Figure A1a, with the result shown in Figure A1c. There are two things to note in this figure that need to be captured in modifications of the CY14 equation to account for a different stress parameter: 1) the curves are independent of $\Delta\sigma$ for frequencies less than the source corner frequencies, and 2) the source corner frequencies vary with $\Delta\sigma$ (such that the high-frequency *FS* is reduced if $\Delta\sigma$ is reduced, and vice versa).

The source scaling for $\Delta\sigma = 50$ bars has been added to Figure A1c, resulting in Figure A1d. The results in the figure show that changes in $\Delta\sigma$ can be captured by changing c_M in equation (A1) to $c_M + \Delta c_M$, so that equation (A1) becomes

$$F_S = c_2(\mathbf{M} - 6) + \frac{c_2 - c_3}{c_n}\ln\left[1 + e^{c_n(c_M + \Delta c_M - \mathbf{M})}\right] \qquad \text{(A2)}$$

While this equation accounts for the stress-parameter dependence of *FS* for large magnitudes, it also includes a stress-parameter dependence of the motion for small magnitudes. This can be seen by taking the asymptotic limit of equation (A2) for $M \ll c_M - \Delta c_M$. Because the CY14

coefficients give $c_n c_M > 10$ for all periods and Δc_M is expected to be relatively small (e.g., -0.2 in Figure A1d) the asymptotic limit of equation (A2) for small **M** becomes

$$F_S \rightarrow c_2(\mathbf{M} - 6) + (c_2 - c_3)(c_M - \mathbf{M}) + (c_2 - c_3)\Delta c_M \quad \text{(A3)}$$

This shows that the last term in equation (A3) needs to be subtracted from equation (A2) in order to remove the stress-parameter dependence of F_S for small **M**. Doing this gives the proper equation for accounting for $\Delta\sigma$ differences by changing c_M, as given in equation (A4):

$$F_S = c_2(\mathbf{M} - 6) + \frac{c_2 - c_3}{c_n}\ln\left[1 + e^{c_n(c_M + \Delta c_M - \mathbf{M})}\right] - (c_2 - c_3)\Delta c_M \quad \text{(A4)}$$

Because applications of equation (A4) will generally involve determinations of $\Delta\sigma$ in host and target regions, the remaining parts of the analysis (1) develop an explicit relation between Δc_M and different $\Delta\sigma$ and then (2) derive adjustments needed to account for the different magnitude scaling of *FS* and *RS*.

Let $\Delta\sigma_1$ and $\Delta\sigma_2$ be the stress parameters in the host and target regions. The equation for the single-corner-frequency source spectrum *E* is

$$E(f) = \frac{C M_0 f^2}{1 + \left(\frac{f}{f_c}\right)^2} \quad \text{(A5)}$$

where C is a constant, M_0 is seismic moment, and the corner frequency f_c is given by

$$f_c = \xi\left(\frac{\Delta\sigma}{M_0}\right)^{\frac{1}{3}} \quad \text{(A6)}$$

where ξ is a constant ($4.906 \times 10^6 \beta_s$, when the units of f_c , $\Delta\sigma$, M_0, and β_s [the shear-wave velocity in the vicinity of the source] are Hz, bars, dyne-cm, and km/s, respectively). The seismic moment M_0 is related to the moment magnitude using equation (A7) (from Hanks and Kanamori, 1979):

$$\log M_0 = 1.5\mathbf{M} + 16.05. \quad \text{(A7)}$$

Following the graphical presentation above, lines are to be fit to $\log E$ vs. **M** for the low- and high portions of **M**, at fixed frequency *f*. The logarithm of equation (A5) is

$$\log E = \log C M_0 f^2 - \log\left[1 + \left(\frac{f}{\xi}\right)^2 \left(\frac{M_0}{\Delta\sigma}\right)^{\frac{2}{3}}\right]. \quad \text{(A8)}$$

In terms of M_0 (to be converted later to **M** using equation (A7)), the low and high magnitude asymptotes of $\log E$ are lines with these equations:

Small M_0:

$$\log E = \log C M_0 f^2 \quad \text{(A9)}$$

Large M_0:

$$\log E = \log C M_0 f^2 - 2\log\left(\frac{f}{\xi}\right) - \frac{2}{3}\log M_0 + \frac{2}{3}\log \Delta\sigma. \quad \text{(A10)}$$

The hinge magnitude (c_M) is the intersection of the two lines; it is determined by equating equations (A9) and (A10), converting M_0 to **M** using equation (A7), and solving for c_M. This results in equation (A11):

$$c_M = \frac{2}{3}\log \Delta\sigma - \frac{2}{3}16.05 - 2\log\frac{f}{\xi} \quad \text{(A11)}$$

The difference in c_M for two values of $\Delta\sigma$ then becomes:

$$\Delta c_{M,FS} = \frac{2}{3}\log\frac{\Delta\sigma_2}{\Delta\sigma_1} \quad \text{(A12)}$$

We added "*FS*" to the subscript of Δc to indicate that the equation applies to the scaling of Fourier spectra, not response spectra. For the graphical example above,

$$\Delta c_{M,FS} = c_{M2} - c_{M1} = \frac{2}{3}\log\frac{50}{100} = -0.20 \quad \text{(A13)}$$

which is the same difference seen in Figure A1d (within roundoff).

MODIFYING THE HINGE MAGNITUDE FOR USE WITH RESPONSE SPECTRA

A modification to equation (A12) is needed the account for differences in the slopes of line segments 1 and 2 for Fourier spectra (*FS*) and for response spectra (*RS*). As shown in Table A1 (where, for convenience, we use notation $s_{1,FS}$, $s_{1,RS}$, $s_{2,FS}$, and $s_{2,RS}$ to indicate the slopes of line segments 1 and 2, for *FS* and for *RS*), the *RS* slopes are always less than the *FS* slopes for all periods. The consequence of using $\Delta c_{M,FS}$ with the *RS* slopes is shown by the dashed lines in Figure A2 for negative and positive changes in c_M. That figure is a schematic representation of the magnitude scaling of the logarithm of a ground-motion intensity measure ($\ln Y$). Because we are only interested in differences in $\ln FS$ and $\ln RS$, we assume in Figure A2 that the segment 1 and segment 2 lines for *FS* and *RS* corresponding to the stress parameter $\Delta\sigma_1$ (the host region) have values of 0.0 at **M**=5.0. The slopes of the *RS* line segments in Figure A2 correspond to the CY14 coefficients for T=0.1 s, but the $\Delta c_{M,FS}$ of ± 0.3 was chosen for the sake of illustrating the discussion here (the actual values of $\Delta c_{M,FS}$ range from -0.15 to +0.06). It is clear from the dashed lines in Figure A2 that using $\Delta c_{M,FS}$ as an adjustment to c_M results in values of $\ln RS$ that are very different than $\ln FS$ for line segment 2. We want to determine a shift $\Delta c_{M,RS}$ such that the change in $\ln RS$ is the same as the change in $\ln FS$ produced by changing the stress parameter from $\Delta\sigma_1$ to $\Delta\sigma_2$. Because the slopes $s_{2,FS}$ and $s_{2,RS}$ are not equal, the change in $\ln FS$ and $\ln RS$ will not be the same for all magnitudes. Our choice for $\Delta c_{M,FS} > 0$ is to find $\Delta c_{M,RS}$ such that the line with the slope $s_{1,RS}$ intersects line segment 2 of the $\ln FS$ function corresponding to $\Delta\sigma_2$. For $\Delta c_{M,FS} < 0$, we choose $\Delta c_{M,RS}$ such that line segment 2 for $\ln RS$ intersects line segment 2 of the $\ln FS$ function at $c_M + \Delta c_{M,FS}$ (see Figure A2).

For $\Delta c_{M,FS} > 0$, the change in $\ln RS$ produced by a shift in the hinge magnitude from c_M to $c_M + \Delta c_{M,RS}$ is

$$\Delta \ln RS = s_{1,RS} \Delta c_{M,RS} \qquad \text{(A14)}$$

and the change in $\ln FS$ for the same shift in the hinge magnitude is given by

$$\Delta \ln FS = s_{1,FS}\Delta c_{M,FS} + s_{2,FS}\left(\Delta c_{M,RS} - \Delta c_{M,FS}\right) \quad \text{(A15)}$$

Equating equations (A14) and (A15) gives the following equation for $\Delta c_{M,RS}$:

$$\Delta c_{M,RS} = \chi_{FS2RS}\Delta c_{M,FS} \quad \text{(A16)}$$

where

$$\chi_{FS2RS} = \frac{s_{1,FS} - s_{2,FS}}{s_{1,RS} - s_{2,FS}} \text{ , for } \Delta c_{M,FS} > 0 \quad \text{(A17)}$$

A similar analysis for $\Delta c_{M,FS} < 0$ finds the same equation for $\Delta c_{M,RS}$ (equation (A16)), but with

$$\chi_{FS2RS} = \frac{s_{1,FS} - s_{2,RS}}{s_{1,RS} - s_{2,RS}} \text{, for } \Delta c_{M,FS} < 0 \quad \text{(A18)}$$

The adjustment to the source function F_S for a host-region $\Delta\sigma_1$ and a target-region $\Delta\sigma_2$ is thus given by equation (A4) with

$$\Delta c_M = \chi_{FS2RS}\frac{2}{3}\log\frac{\Delta\sigma_2}{\Delta\sigma_1} \quad \text{(A19)}$$

where χ_{FS2RS} is given either by equation (17) or (18), depending on the sign of $\Delta c_{M,FS}$ (equation (A12).

The revised ln *Y* corresponding to a change in the stress parameters is now shown by the solid *RS* lines in Figure A2. Table A1 gives χ_{FS2RS} for the CY14 ground-motion prediction model.

Appendix Table

Table A1. For a single corner frequency, constant stress parameter source model, $s_{1,FS} = 1.5 \ln 10 = 3.454$ and $s_{2,FS} = 0.5 \ln 10 = 1.151$. $s_{1,RS}$ and $s_{2,RS}$ are the CY14 coefficients c_3 and c_2, respectively.

T (s)	$s_{1,FS}$	$s_{1,RS}$	$s_{2,FS}$	$s_{2,RS}$	χ_{FS2RS}	
					$\Delta c_{M,FS} < 0$	$\Delta c_{M,FS} > 0$
0.010	3.454	1.964	1.151	1.060	2.649	2.835
0.020	3.454	1.964	1.151	1.060	2.649	2.835
0.030	3.454	1.964	1.151	1.060	2.649	2.835
0.040	3.454	1.964	1.151	1.060	2.649	2.835
0.050	3.454	1.964	1.151	1.060	2.649	2.835
0.075	3.454	1.964	1.151	1.060	2.649	2.835
0.100	3.454	1.964	1.151	1.060	2.649	2.835
0.150	3.454	2.036	1.151	1.060	2.452	2.602
0.200	3.454	2.152	1.151	1.060	2.192	2.301
0.300	3.454	2.344	1.151	1.060	1.864	1.931
0.400	3.454	2.471	1.151	1.060	1.697	1.745
0.500	3.454	2.557	1.151	1.060	1.599	1.638
0.750	3.454	2.681	1.151	1.060	1.477	1.505
1.000	3.454	2.747	1.151	1.060	1.419	1.443
1.500	3.454	2.816	1.151	1.060	1.363	1.383
2.000	3.454	2.851	1.151	1.060	1.336	1.354
3.000	3.454	2.888	1.151	1.060	1.310	1.326
5.000	3.454	2.917	1.151	1.060	1.289	1.304
7.500	3.454	2.932	1.151	1.060	1.279	1.293
10.000	3.454	2.940	1.151	1.060	1.274	1.288

Appendix Figures

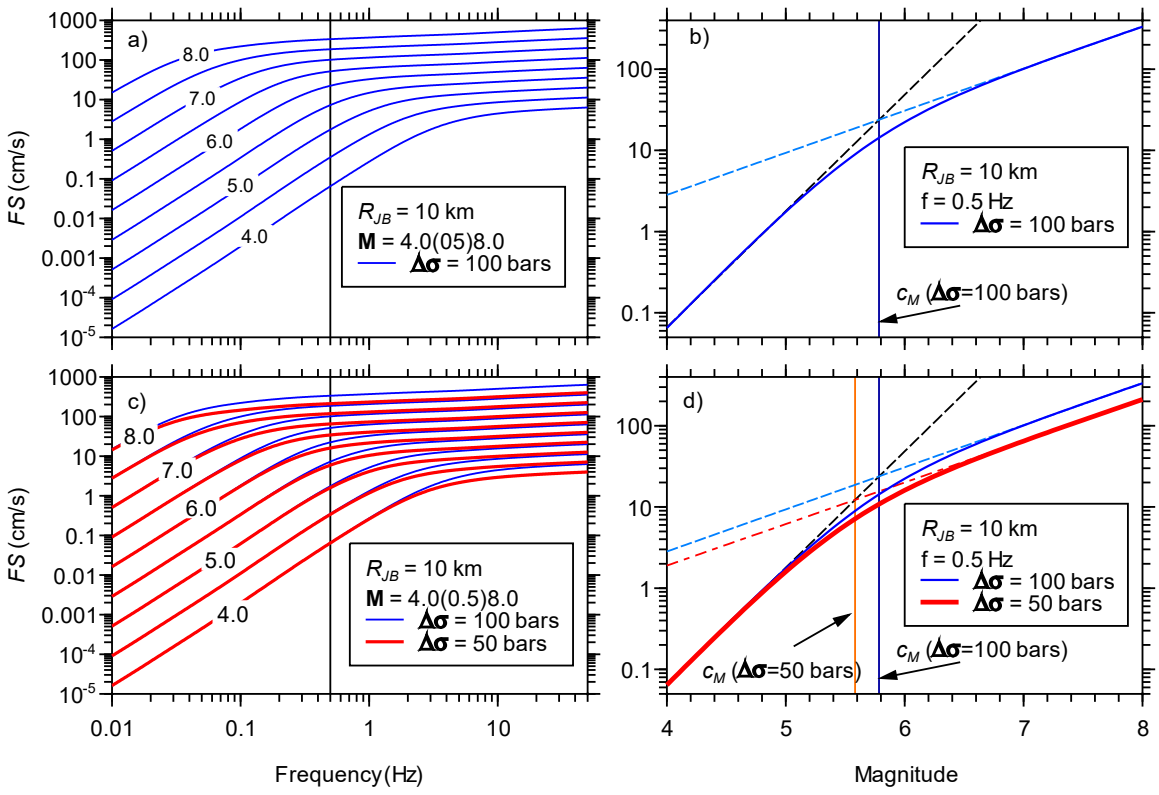

Figure A1. Illustration of the dependence of the magnitude scaling on the stress parameter $\Delta\sigma$ (see text for discussion of the various parts of the figure). As a side note, the *FS* in parts a) and c) rises slowly at high frequencies rather than being flat, as implied by equation (A5), because the Al Atik and Abrahamson (2021) crustal amplifications, which increase with frequency, have been included (and $\kappa_0 = 0$ s, so the *FS* at high frequencies is not reduced).

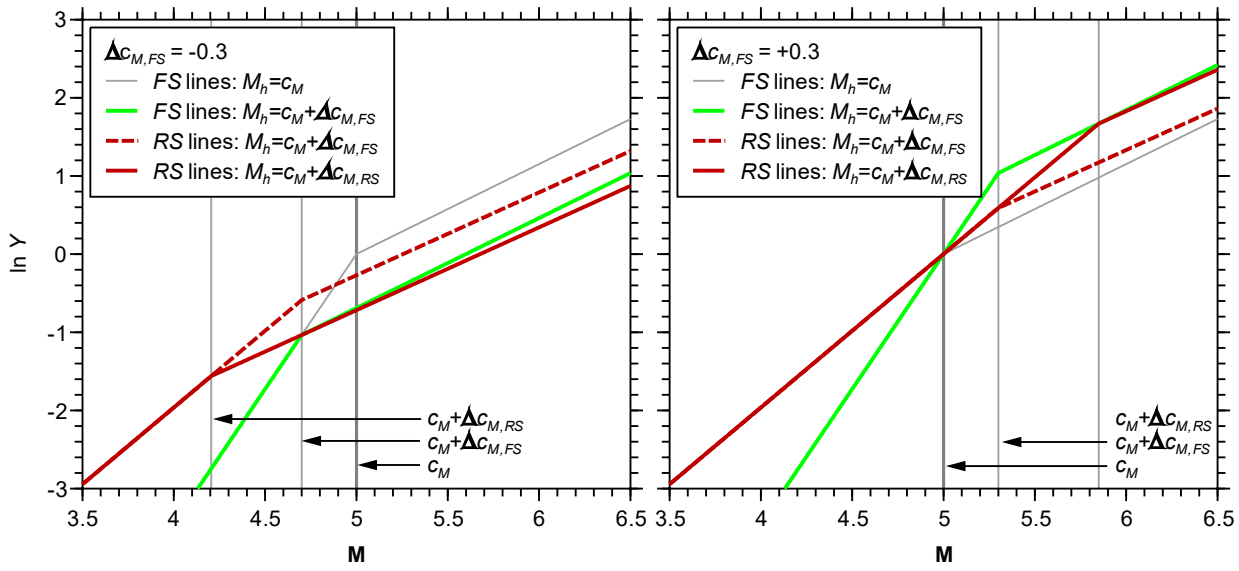

Figure A2. Illustrating the scaling of Fourier spectra (*FS*) and response spectra (*RS*) for negative (left side) and positive (right side) shifts in $\Delta c_{M,FS}$, showing that the shift in $\Delta c_{M,RS}$ needs to be modified from that for $\Delta c_{M,FS}$ in order for the *RS* amplitude of line-segment 2 to be similar to that of the *FS* line-segment 2 amplitude.